ANALYSIS OF PHOTORECEPTOR OUTER SEGMENT MORPHOGENESIS IN ZEBRAFISH IFT57, IFT88 AND IFT172 INTRAFLAGELLAR TRANSPORT MUTANTS

A Thesis

by

SUJITA SUKUMARAN

Submitted to the Office of Graduate Studies of
Texas A&M University
in partial fulfillment of the requirements for the degree of

MASTER OF SCIENCE

December 2008

Major Subject: Biology

ANALYSIS OF PHOTORECEPTOR OUTER SEGMENT MORPHOGENESIS IN ZEBRAFISH IFT57, IFT88 AND IFT172 INTRAFLAGELLAR TRANSPORT MUTANTS

A Thesis

by

SUJITA SUKUMARAN

Submitted to the Office of Graduate Studies of
Texas A&M University
in partial fulfillment of the requirements for the degree of

MASTER OF SCIENCE

Approved by:

Chair of Committee,	Brian D. Perkins
Committee Members,	Bruce Riley
	Tina L. Gumienny
Head of Department,	Thomas McKnight

December 2008

Major Subject: Biology

ABSTRACT

Analysis of Photoreceptor Outer Segment Morphogenesis in Zebrafish IFT57, IFT88 and IFT172 Intraflagellar Transport Mutants. (December 2008)

Sujita Sukumaran, B.S., Birla Institute of Technology and Science

Chair of Advisory Committee: Dr. Brian D. Perkins

Vertebrate photoreceptors are polarized cells that consist of a specialized sensory structure termed the outer segment required for phototransduction and an inner segment that contains the cellular organelles. Proteins synthesized in the inner segment are transported to the outer segment via a connecting cilium by a process called Intraflagellar Transport (IFT). The IFT mechanism refers to the movement of a multi-subunit complex along the flagellar axoneme, and mutations in some IFT components cause retinal degeneration. To better understand the role of IFT in early photoreceptor development, we studied zebrafish with mutations in genes encoding three specific subunits of the IFT particle: IFT57, IFT88 and IFT172. These mutants exhibit photoreceptor defects by five days post fertilization (dpf); however, it is not known whether outer segment formation initiates at earlier time points and then degeneration occurs or if outer segments never form at all. To understand this, we performed transmission electron microscopy to study the ultrastructure of photoreceptors at 60, 72 and 96 hours post fertilization (hpf).

At 60 hpf, developing outer segments were seen in IFT57 mutant and wild type embryos, however, disorganized membranous structures were observed in IFT88 and IFT172 mutants. At 72 hpf, the number of outer segments in the IFT57 mutants was reduced by 88% when compared to wild type, indicating a defect in initiation of outer segment formation. By 96 hpf we see a reduction in both outer segment length and number in IFT57 mutants. In comparison, the IFT88 and IFT172 mutants do not grow outer segments at any time point. To complement our ultrastructural analysis, we performed immunohistochemistry to understand cell morphology and protein trafficking in these mutants. Zpr1, a marker for cone morphology, showed the presence of normal cones initially that began to degenerate at later time points. Immunohistochemistry with rhodopsin, a phototransduction protein that localizes to the outer segment, revealed that rhodopsin was mislocalized in all the three mutants by 96 hpf. Connecting cilia labeled with acetylated tubulin were highly reduced in IFT57 mutants whereas none were observed in IFT88 and IFT172 mutants. Together these data indicate that IFT57 is required for maintenance and growth of outer segments whereas IFT88 and IFT172 are required for initiating outer segment formation.

DEDICATION

To my family and friends

ACKNOWLEDGEMENTS

I would like to express my heartfelt gratitude to my mentor, Dr. Brian Perkins for giving me the opportunity to work in his laboratory. He has been very instrumental in the development of my scientific thinking and I would like to thank him for his support and guidance throughout the course of my research at Texas A&M University. My gratitude also goes out to my committee members, Dr. Bruce Riley and Dr. Tina Gumienny for their insightful comments and suggestions.

This work could not have possible without Bryan Krock. I am forever indebted to him for many things, especially protocols, literature reviews and of course the expansion my "American" vocabulary. Additionally, I would like to thank Shannon Lunt for always being there both professionally and personally. Both Bryan and Shannon have been very patient in reading numerous drafts of my thesis and manuscript, for which I am very grateful. I would also like to thank Leah, Chace, Pedro, Ethan and the undergrads at the lab for all the good times and laughs. My gratitude also goes out to Ann Ellis for sharing her expertise in electron microscopy. She has been very patient in teaching me the technique and helping me troubleshoot protocols.

I would like to thank my family for their unconditional love, support and prayers, which has made me the person that I am today. My gratitude also goes out to my roommates, friends at FQ and College Main for the all the good times and fun. Finally, I would like to thank Sona, Raghav, Uzaira and Anand for their unfaltering support and encouragement during the course of my graduate study.

NOMENCLATURE

BBS	Bardet Biedl Syndrome
CHE	Chemotaxis
Daf-d	Dauer abnormal formation-defective
dpf	Days post fertilization
Dyf	Dye filling defective
EDTA	Ethylene diamine tetra-acetic acid
ERG	Electroretinogram
GCL	Ganglion cell layer
HD	Huntington disease
hpf	Hours post fertilization
IFT	Intraflagellar transport
ips	Interphotoreceptor space
INL	Inner nuclear layer
IPL	Inner plexiform layer
JATD	Jeunes asphyxiating thoracic dystrophy
Mchr1	Melanin concentrating hormone 1
OKR	Optokinetic response
ONL	Outer nuclear layer
OPL	Outer plexiform layer
OS	Outer segment
OSM	Osmotic avoidance

PBS	Phosphate buffered saline
PKD	Polycystic kidney disease
RPE	Retinal pigment epithelium
SDS	Sodium dodecyl sulfate
Sstr3	Somatostatin receptor 3
SS	Somite stage
TEM	Transmission electron microscopy

TABLE OF CONTENTS

Page

LIST OF FIGURES

Page

1. INTRODUCTION

1.1. Eye morphogenesis

Understanding neural systems and the behavior of individual nerve cells has been a topic of intense research for several decades (Eisen, 1991). The retina, a light sensing visual organ derived from the forebrain has been found to be the most accessible source for understanding basic neural mechanisms and processing that can be related to the vertebrate brain (Dowling, 1987). Several decades of research has led to the identification of zebrafish as an excellent model system for studying retinal architecture and development (Fadool & Dowling, 2008). Eye morphogenesis in zebrafish begins at the six somite stage (SS) with the evagination of the optic primordia, a solid mass of cells from the forebrain (Schmitt & Dowling, 1994). About two-thirds of this mass begins to separate from the forebrain forming a narrow optic stalk at the anterior end between 10-12 SS (~14-15 hpf). Cells from the center of each optic primordia invaginate by 17-18 SS, leading to the formation of prominent optic cups by 18 SS. During this period, two conspicuous grooves develop at the dorsal and ventral pole of the eye cup called the posterior and choroid fissure, respectively. The choroid fissure is a prominent furrow that lies adjacent to the optic stalk and is covered by mesenchyme and ligaments at 36 hpf (Schmitt & Dowling, 1994). Along with these structural changes in the forebrain, cells begin differentiate and adopt specific fates, giving rise to multiple layers of the eye.

This thesis follows the style of *Vision Research*.

1.2. The retina

The vertebrate retina is a complex organ made up of different types of neurons (Dowling, 1987). The cell bodies of these neurons are organized to form three distinct nuclear layers that are connected to each other through their synapses, forming two separate plexiform layers (Kolb & West, 1977). The nuclear layers are oriented with respect to the lens as the ganglion cell layer (GCL), inner nuclear layer (INL) and outer nuclear layer (ONL) or photoreceptor layer. The inner plexiform layer (IPL) lies between the GCL and INL and the outer plexiform layer (OPL) is between the INL and ONL (Fig. 1) (Dowling, 1970, Haycock & Bro, 1975). The outermost limiting layer lining the retina is called the retinal pigment epithelium (RPE).

Right behind the lens, the nuclei of the ganglion cells form the most proximal layer with their axonal projections collectively exiting the eye as the optic nerve (Dowling, 1970). Next is the inner nuclear layer, consisting of the bipolar, horizontal, amacrine and Müller cells (Kolb, Nelson & Mariani, 1981). The bipolar cells extend processes to both the IPL and OPL and are output neurons carrying signals from the OPL to the IPL (Fig. 1). The horizontal cell bodies are located towards the distal margin of the inner nuclear layer and mediate lateral interactions by sending processes out only to the OPL. The amacrine cells are arranged along the proximal border of the inner nuclear layer; their processes are confined to the IPL, thereby controlling lateral interactions similar to the horizontal cells. Müller cells are the predominant type of glial cells that extend across the retina from the outer to the inner nuclear layer. They have several functions that involve protecting, nourishing and providing support to the

neurons. The outer nuclear layer (OPL) is made of rods and cones that mediate dim light and color vision, respectively (Dowling, 1987, Kolb, 1977). The RPE interdigitates with the photoreceptors and serves multiple functions such as: providing trophic support for the photoreceptor outer segments, preventing the scattering of light and recycling the chromophore, retinal (Marmorstein, 2001, Strauss, 2005, Young, 1971).

Light entering through the lens passes through the transparent retina and causes hyperpolarization of the photoreceptors (Dowling, 1978). Optical quality is enhanced by the presence of melanin, a pigment molecule present in the RPE, which aids in absorption of scattered light. The visual responses generated by the photoreceptors are then transmitted to the GCL via the INL. Hence the synaptic connections between the different classes of neurons serve to form a continuous network that transmits all visual information to the brain.

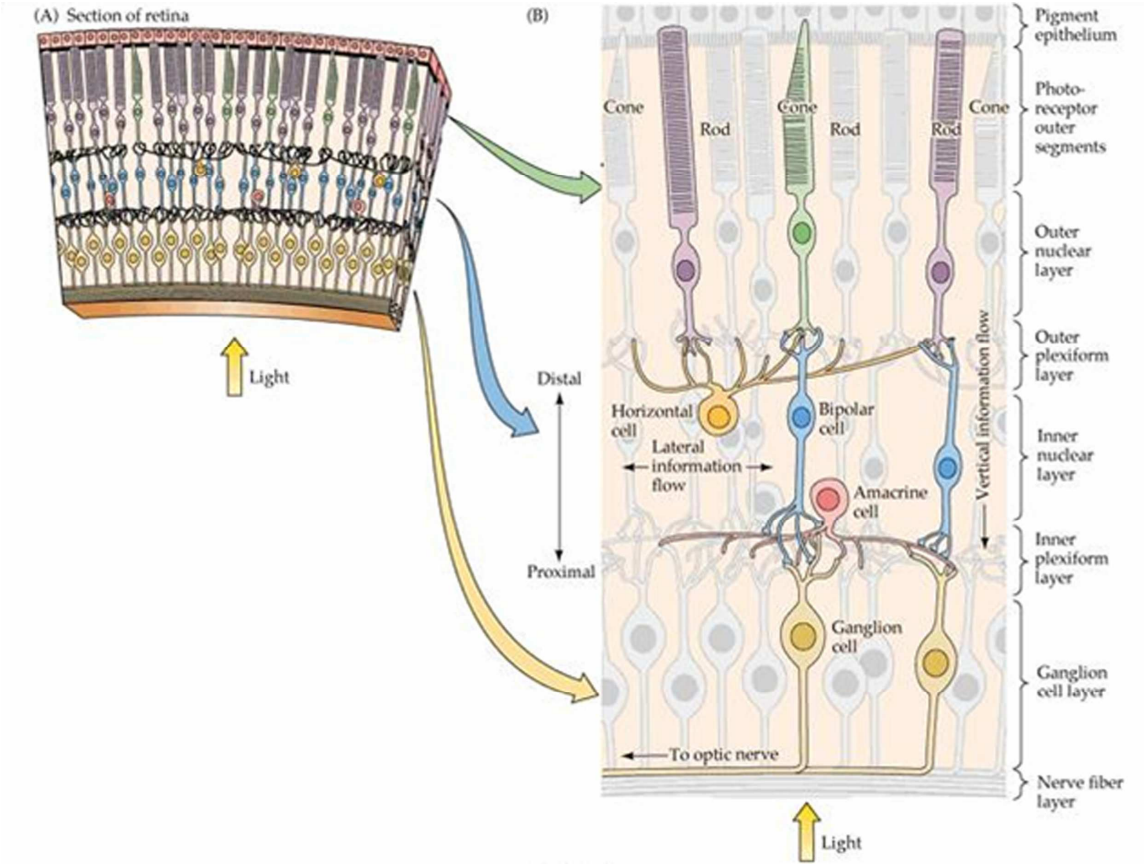

Figure 1. The layers of the retina.

The retina is made up of three nuclear (GCL, INL, ONL) and two plexiform layers (IPL and OPL). *Adapted from Christine Dahlquist, Color Perception and the Human Body, 2007.*

1.3. Retinal neurogenesis

The various cell types of the retina differentiate at specific time points and this has been well defined in zebrafish. The first postmitotic neuron originates in the GCL at 28 hpf (hours post fertilization), followed by differentiation of INL and ONL neurons at 43 hpf and 54 hpf, respectively (Easter & Nicola, 1996, Hu & Easter, 1999). Interestingly, retinal differentiation in other vertebrates like chick, frog, mouse and

human begins at the center and progresses to the periphery (Kahn, 1974, Schmitt & Dowling, 1996, Young, 1985). Zebrafish photoreceptors, on the other hand, begin to differentiate at 50 hpf in a region that is nasal to the optic nerve, termed the ventral patch. Following this, cone differentiation spreads in a wave like fashion further into the nasal region by 54 hpf and then simultaneously into the central and temporal retina by 56 hpf (Raymond, Barthel & Curran, 1995). The first rods also appear in the ventral patch, but unlike cones, exhibit a scattered distribution pattern, beginning nasal to the choroid fissure and then moving to the temporal side during this same time period (Raymond et al., 1995, Schmitt & Dowling, 1996). Ultimately, a functional eye is observed at approximately 72 hpf when zebrafish larvae display behavioral responses to light (Easter & Nicola, 1996).

1.4. Photoreceptor morphology

Rods and cones possess a highly polarized morphology consisting of an inner and outer segment region linked by a narrow cilium (Fig. 2). The inner segment consists of cellular organelles such as the mitochondria, Golgi apparatus, endoplasmic reticulum and nucleus. The outer segment (OS) is the region where phototransduction occurs and consists of stacked discs that are continuously formed at the base and move towards the apical end. The outer segment is made up of about 50% protein and 50% lipid (Anderson & Maude, 1970, Basinger, Bok & Hall, 1976). Rhodopsin, a G-protein coupled receptor and an important visual pigment molecule, constitutes 90% of the outer segment protein composition. Approximately 10% of the outer segment is shed on a daily basis which is phagocytosed by the RPE (Young, 1967). However, the outer

segment lacks cellular organelles required for protein and membrane synthesis. Hence it has to depend on the inner segment for replacement of the lost material (Young, 1967).

1.5. Cilia

Proteins synthesized in the inner segment have to pass through a narrow connecting cilium on their way to the outer segment. In a broader sense, cilia are classified into two kinds; motile or non-motile cilia. Motile cilia have a 9+2 structure with nine outer doublet microtubules surrounding a central pair, whereas non-motile cilia lack the central microtubular singlets (9+0). Motile cilia are found on the respiratory tract, testes, oviduct, olfactory and ependymal cells of the brain (Afzelius, 2004, Odor & Blandau, 1985, Sanderson & Sleigh, 1981). Rudimentary cilia, primary cilia and photoreceptor cilia are examples of non-motile cilia found in various tissues such as neurons, glial cells, chondrocytes and retina (Afzelius, 2004, Pazour & Witman, 2000). Nodal cilia present on the embryonic node in the gastrulation stage move in a propeller-like fashion and are the only known exception of primary cilia that can move (Nonaka et al., 1998). Hence, nodal cilia are now beginning to be classified into a separate category itself. Altogether these different kinds of cilia are present on almost all cell types in the body (Davenport & Yoder, 2005).

Functionally, motile cilia aid in the movement of extracellular fluid of the environment that they project into, whereas non-motile cilia primarily serve as sensory organelles. Transmembrane receptors like Somatostatin receptor 3, Smoothened and polycystins localize to the cilia and it is likely that these receptors are responsible for the sensory perception observed in these sensory, non-motile cilia (more details in Section

1.11) (Corbit et al., 2005, Handel et al., 1999, Pazour et al., 2002b). As mentioned earlier, the connecting cilium in a photoreceptor is non-motile with a 9+0 microtubule structure (Fawcett & Porter, 1954). The connecting cilium can be classified as having three distinct regions; an upper axoneme that is continuous with the outer segment, a middle part that is surrounded by surface membrane, and a lower portion that is attached to the basal body. The basal body is a centriole-like structure present at the apical end of the inner segment (De Robertis, 1956a).

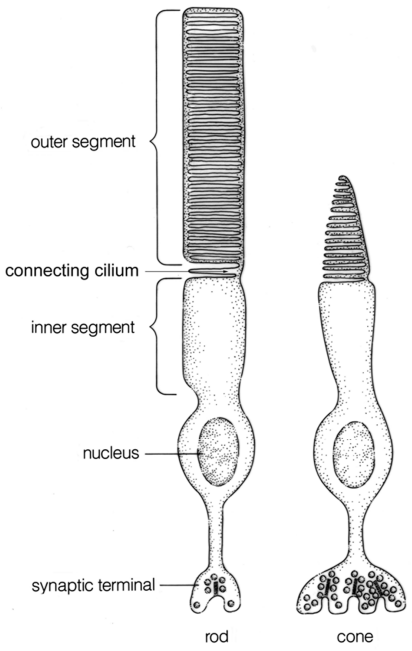

Figure 2. Rod and cone morphology.

Rods and cones are highly polarized structures consisting of an inner segment, outer segment, connecting cilium and synaptic termini. *Adapted from De Robertis, 1960.*

1.6. Stages of outer segment formation

In the retinas of rat and mice there are certain characteristic developmental changes that occur between the time they are born and the 18th day after birth (De Robertis, 1960). These changes have been classified into three main stages and show that the outer segment is essentially a modified sensory cilium (De Robertis, 1956c). The initial stage of photoreceptor development is characterized by a cilium projecting from a bulge of protoplasm of the inner segment. The second stage is characterized by the enlargement of the apical end of this primitive cilium due to the accumulation of "morphogenetic material" that consists of short pieces of microtubules and vesicles (De Robertis, 1956c). Finally, primitive rod and cone sacs replace the morphogenetic material and align transverse to the surface membrane. The basal part of the cilium however, remains undifferentiated with the 9+0 microtubule structure and is continuous with the basal body (Fig. 3) (De Robertis, 1956c, Horst, Johnson & Besharse, 1990). Additionally, electron microscopy data in zebrafish have shown that these microtubule doublets extend into the OS and transition into singlets towards the distal end (Insinna et al., 2008). These morphogenetic observations confirm that in vertebrates, the outer segment is an extension of the connecting cilium. As a result, the outer segment requires the transport of ciliary components like tubulin essential for its structure in addition to phototransduction proteins (Mendez, Lem, Simon & Chen, 2003, Perkins, Fadool & Dowling, 2004, Peterson et al., 2003).

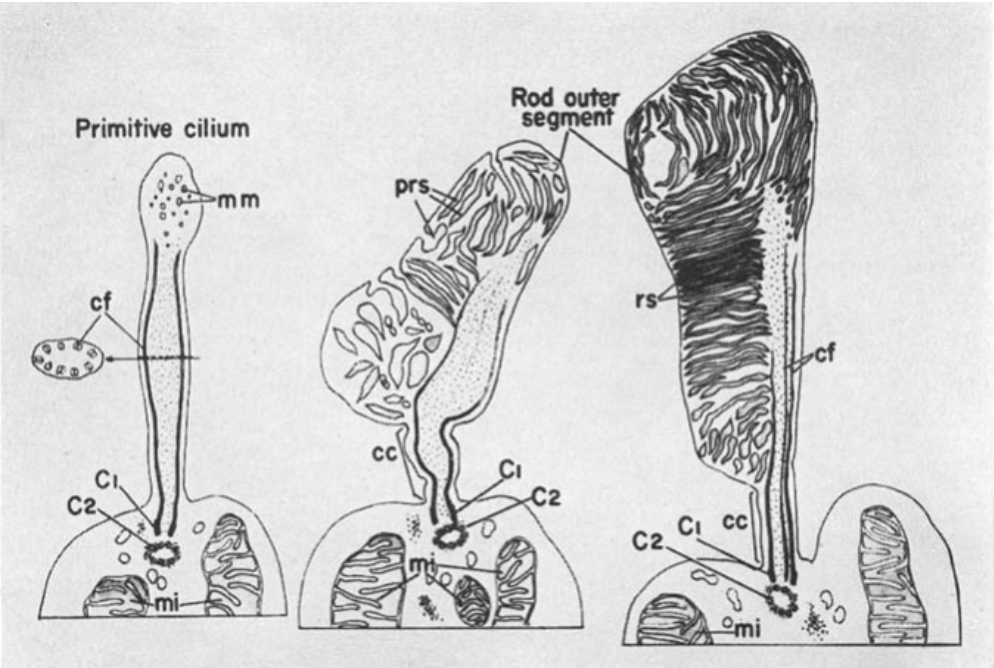

Figure 3. Stages of outer segment development.

The apical end of the primary cilium forms a bulge initially that gets filled with membrane and protein material. Primitive rod sacs (prs) organize into discs and are arranged transverse to the membrane. The basal part of primitive cilium extends into the outer segment as the ciliary filament (cf) and is also continuous with the basal body. mm, morphogenetic material; C1 and C2, the two centrioles that form the basal body; mi, mitochondria; cc, connecting cilium; rs, rod sacs. *Adapted from De Robertis, 1960.*

1.7. Intraflagellar transport

Protein trafficking via the connecting cilium is mediated by a process known as the Intraflagellar transport mechanism (IFT). IFT was discovered in the unicellular biflagellate organism, *Chlamydomonas*, as the movement of granule-like particles along the length of the flagella (Kozminski, Johnson, Forscher & Rosenbaum, 1993). These

particles appear as rafts between the doublet microtubules and flagellar membrane, when visualized by electron microscopy. As the photoreceptor connecting cilium is similar to the flagella observed in *Chlamydomonas*, it was hypothesized that protein transport across this structure is regulated by IFT[1] (Rosenbaum, Cole & Diener, 1999).

The IFT particle is a multi-protein complex made up of 15-17 polypeptides (Piperno & Mead, 1997). Biochemical characterization of this particle showed that it can be separated into two subcomplexes (complex A and B) based on sucrose density gradient centrifugation (Cole et al., 1998). Complex A and B are made up of at least 5 and 10 polypeptide subunits, respectively (Fig. 4). Bioinformatics has revealed that the protein-protein interaction domains, like tetratricopeptide repeats (TPR), WD40 repeats and coiled coil domains, enable these subunits to form a complex (Lamb, Tugendreich & Hieter, 1995, Pedersen et al., 2005). TPR and WD40 domains mediate transient interactions required for the binding of these subunits to one another and also to cargo. Coiled coil domains on the other hand are required for longer, stable interactions seen in the tetrameric complex formed between two subunits of IFT81 and IFT72/74. This oligomer in turn forms a 500-kDa core made up of IFT88, IFT81, IFT74/72, IFT52, IFT46 and IFT27, which does not dissociate even at high ionic strength washes (Lucker et al., 2005).

Further studies to understand the localization patterns of the IFT components in *Chlamydomonas* showed that subunits, like IFT172, IFT139, IFT81, IFT57 and IFT52

[1] Cilia are shorter and more in number on the cell surface when compared to flagella. However, they have a similar structure which is conserved among eukaryotes and hence these terms can be used interchangeably.

localize largely to the cell body with a small amount in the flagella (Cole et al., 1998). A similar distribution pattern for IFT52, IFT20 and IFT88 was observed in cultured mammalian cell lines (Deane et al., 2001, Robert et al., 2007). It is speculated that the localization of IFT subunits and cargo to the base of the cilium represents a cytoplasmic pool of individual components (Follit, Tuft, Fogarty & Pazour, 2006). It is from this pool that cargo and flagellar precursors destined to the outer segment assemble with the IFT subunits to form a complex that is transported.

Complex	IFT Particle Peptides
Complex A	IFT144
	IFT140
	IFT139
	IFT122
	IFT43
Complex B	IFT172
	IFT88
	IFT81
	IFT80
	IFT74
	IFT57
	IFT52
	IFT46
	IFT27
	IFT20

Figure 4. Components of the IFT complex.

The IFT particle can be separated in to two sub-complexes: Complex A and Complex B. *Adapted from Cole et al., 1998.*

1.8. Motors of the IFT complex

The movement of IFT particles along the doublet microtubules of the axoneme is mediated by two motors; kinesin II and cytoplasmic dynein 2 (Fig. 5). Anterograde movement towards the tip of the flagellum requires heterotrimeric kinesin II which has two motor subunits, KIF3A and KIF3B and one accessory subunit, KAP (Kondo et al., 1994, Yamazaki, Nakata, Okada & Hirokawa, 1995). Kinesin II was discovered in *Chlamydomonas* as the FLA10 gene that is required for anterograde transport. *fla10*^{ts} mutants that lack a functional kinesin II protein at the restrictive temperature lose flagella and their ability to transport IFT particles (Kozminski, Beech & Rosenbaum, 1995, Walther, Vashishtha & Hall, 1994). The discovery of this mutant was a major step toward the classification of the various subunits of the IFT complex, and it was achieved by the comparison of flagellar extracts from *fla10* mutants grown at permissive and restrictive temperatures (Cole et al., 1998).

As expected, kinesin II co-immunoprecipitated with IFT proteins in the photoreceptor (Baker et al., 2003, Krock & Perkins, 2008). It has been shown that kinesin II directly binds to IFT20 and requires ATP in order to be released from the complex at the flagella tip. However**,** in the absence of IFT20, kinesin II is still bound to the complex, suggesting the presence of another putative protein responsible for this association (Krock & Perkins, 2008). This has led to the speculation that the IFT20-Kinesin II link is essential for the ATP- dependent release of kinesin II at the tip of the flagella.

Additional kinesin motors, such as OSM-3 identified in *C.elegans*, function redundantly with kinesin II for regulating anterograde movement of the IFT particle along the initial doublet axoneme. Moreover, OSM-3 alone is required for extension of distal singlet microtubules in sensory neurons (Snow et al., 2004). Kif17, a zebrafish homologue of OSM-3, co-immunoprecipitates with IFT proteins like IFT20, IFT57 and IFT88 (Insinna et al., 2008). Additionally, Kif17 is localized along the ciliary axoneme in photoreceptors. Lack of Kif17 resulted in disruption of OS formation and protein trafficking, indicating the importance of all the kinesin components for anterograde transport (Insinna et al., 2008).

Retrograde movement is mediated by cytoplasmic dynein 2, which is associated with accessory subunits including light intermediate chains (LIC), intermediate chains (IC) and light chains (LC) (Tynan, Gee & Vallee, 2000). *Chlamydomonas* mutants for the dynein heavy chain, cytoplasmic dynein 1b, are characterized by short, stumpy flagella that have normal anterograde transport. As expected, the stumpy flagella observed in these retrograde mutants consist of IFT components, radial spokes, microtubules and other components that are trafficked normally to the flagella (Pazour, Dickert & Witman, 1999, Porter et al., 1999). Similarly, mutation in the dynein light chain, LC8 in *Chlamydomonas* shows a similar phenotype, highlighting that these different components work in concert to form a dynein complex that regulates retrograde transport in the flagella (Pazour, Wilkerson & Witman, 1998).

Furthermore, several mutant studies have helped in understanding the specific interaction of these motors with the IFT complex. It has been shown that complex B

mutants mostly lack flagella, similar to the phenotype seen in kinesin mutants (Pazour et al., 2000). Similarly, complex A and dynein mutants possess similar phenotypes of short, stumpy flagella implying the requirement of complex A in retrograde transport (Piperno et al., 1998). These data indicate the involvement of complex A and B in retrograde and anterograde transport, respectively. However, except for the IFT20-kinesin II link, there is no evidence of a direct interaction by the other IFT components with either of the motors.

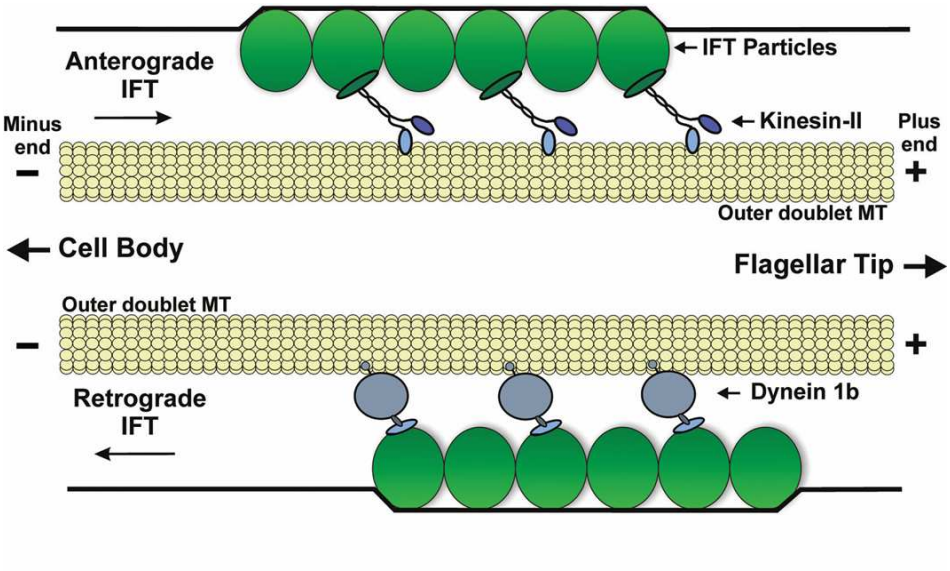

Figure 5. The Intraflagellar transport mechanism.

The cargo interacts with the IFT complex and is carried towards the flagellar tip by Kinesin II. At the tip, motors are switched and dynein brings the components back to the cytoplasm. *Adapted from Pazour and Rosenbaum, Trends in Cell Biology, 2002.*

1.9. Cargo transported by the IFT complex

Very little is known about cargo directly transported by the IFT complex. Few cargo components, such as outer dynein arms, radial spokes and components of the axoneme, have been identified in pull down assays with IFT complex (Hou et al., 2007, Qin et al., 2004). The discovery of a direct link with predicted cargo components such as phototransduction proteins remains unidentified. Mutations in Kif3A and several IFT components are accompanied by rhodopsin mislocalization, strongly suggesting that rhodopsin is a potential cargo component (Marszalek et al., 2000, Tsujikawa & Malicki, 2004).

In addition to the transport of these cargo molecules, there is increasing evidence that signaling pathways require IFT for early development and organogenesis. Zebrafish that lack IFT46 are dorsalized with their notochord broadened and tail extending prematurely off the yolk (Gouttenoire et al., 2007). These phenotypes are similar to mutants of the BMP pathway, suggesting that IFT46 is required for normal BMP signaling in zebrafish (Gouttenoire et al., 2007). The mouse null mutants *hippi, flexo* and *wimple,* which encode IFT57, IFT88 and IFT172 respectively, cause defects in left-right patterning and Shh signaling, implicating a potential role for IFT in the Hedgehog pathway (Houde et al., 2006, Huangfu et al., 2003).

1.10. Intraflagellar transport mutants

The sequence of IFT subunits identified in *Chlamydomonas* has formed the basis for identification of their homologs across several species. An insertional mutagenesis screen that isolated *Chlamydomonas* mutants defective in flagella identified several

components of the IFT complex (Pazour & Witman, 2000). *Chlamydomonas* IFT57 mutants possess short flagella whereas IFT52, IFT88, IFT140 and IFT172 mutants were completely bald (Cole, 2003).

Many of the IFT homologs in worms were identified through BLAST searches of *C.elegans* genome against that of *Chlamydomonas* and higher organisms (Cole et al., 1998, Haycraft et al., 2003, Haycraft et al., 2001, Tsujikawa & Malicki, 2004). In *C.elegans,* cilia are present only on 60 out of the 302 neurons present in the nervous system and defects in cilia structure affect sensory cells such as the amphids, phasmids, inner and outer labials. Coincidentally, several IFT homologs, OSM-5 (IFT88), OSM-1 (IFT172), OSM-6 (IFT52), CHE-13 (IFT57), are expressed in these sensory neurons (Haycraft et al., 2003, Haycraft et al., 2001). *C.elegans* that possess mutations for these IFT subunits display disrupted sensory cilia resulting in defects in osmotic avoidance (Osm), chemotaxis (Che), dauer formation (Daf-d), fluorescent dye uptake (Dyf), male mating behavior and egg laying, which are characteristic phenotypes observed in IFT mutants (Apfeld & Kenyon, 1999).

As cilia are present on almost all cell types in higher organisms, it is not surprising that mutations in IFT cause defects in photoreceptors, kidney, nodal cilia, olfactory neurons and sensory hair cells of the inner ear (Pazour & Rosenbaum, 2002, Tsujikawa & Malicki, 2004). The identification of IFT mutants in zebrafish began with a large-scale retroviral mutagenesis screen that identified 315 mutations that had obvious phenotypes representing individual organ system development (Amsterdam & Hopkins, 1999). Screening through these mutants led to the identification of IFT57, IFT81 and

IFT172 subunits, as zebrafish that had mutations for these polypeptides developed kidney cysts (Sun et al., 2004). Similarly, IFT57 and IFT172 were identified from the same collection of mutants where the selection was based on a phenotype where photoreceptor development and survival were severely affected (Gross et al., 2005). The IFT88 gene in zebrafish was identified in an independent study as the *oval* allele (Tsujikawa & Malicki, 2004). These mutants were characterized by loss of cilia from the retina, auditory hair cells and olfactory sensory neurons. Conversely, in the same study, morpholino knockdown of IFT140, a subunit in complex A, displayed a very mild phenotype in which the zebrafish were barely affected (Tsujikawa & Malicki, 2004). Studies in *C.elegans* also show similar results, wherein cilia are of normal length in complex A mutants (Perkins, Hedgecock, Thomson & Culotti, 1986). Together these data suggest that complex B plays a more prominent role in cilia since loss of its components results in phenotypes that are more severe when compared to lack of complex A.

Finally, analysis of IFT mutants in mice showed drastic phenotypes. As mentioned earlier, *hippi*, *flexo* and *wimple*, the mouse homologs of IFT57, IFT88 and IFT172, are embryonic lethal resulting in death by mid-gestation (Houde et al., 2006, Huangfu et al., 2003). Early death of mice prevents an in-depth understanding of the role of IFT in mouse photoreceptors. Hence the retroviral insertion in zebrafish has proven to be beneficial in investigating the consequences of IFT defects in the eye, kidney, node and brain (Gross et al., 2005). Studies from different model systems has

made it clear that IFT is a well conserved process across several ciliated species ranging from nematodes to vertebrates (Rosenbaum & Witman, 2002).

Interestingly, analysis of individual IFT subunits has now made it apparent that all tissues in an animal model are not equally affected in a particular IFT mutant. For instance, IFT81 mutants have normal photoreceptors but develop kidney cysts (Gross et al., 2005). Loss of Kif17, the zebrafish homolog of OSM-3, causes photoreceptor outer segment defects but motile cilia in kidneys remain normal (Insinna et al., 2008). Apart from their obvious role in cilia, some IFT components have been shown to have other functions. IFT27 is a Rab-like G protein required for cell-cycle control as partial knockdown of IFT27 results in elongation of the cell cycle (Qin, Wang, Diener & Rosenbaum, 2007). IFT20 is present in the golgi complex in addition to being localized to the basal body and cilium, suggesting that IFT20 could aid in the transport of ciliary proteins from the golgi to cilia. Moderate knock down of IFT20 reduces the amount of polycystin-2, a transmembrane protein trafficked to the cilium (Follit et al., 2006). These data highlight that IFT components possess additional roles that are yet to be identified and characterized.

1.11. Cilia dependent diseases and disorders

Defects in cilia, collectively named ciliopathies, have profound effects during early development and physiology of several organ systems. Many higher organism IFT mutants like mice and zebrafish develop kidney cysts and situs inversus, which are phenotypes also seen in humans. It has been established that renal cysts observed in individuals with polycystic kidney disease (PKD) occur due to over-proliferation of

renal epithelial cells when cilia are absent. Transmembrane proteins like polycystin 1 and polycystin 2 localize to the cilia and act as mechanosensors that control proliferation and differentiation of renal cells (Pazour et al., 2002b, Yoder, Hou & Guay-Woodford, 2002). As a result, absence of cilia causes mislocalization of the factors that control cell proliferation resulting in kidney cysts. In addition to their role in formation of kidney cysts, cilia have been implicated to be involved in left-right asymmetry defects. Cilia present on the embryonic node rotate in a clockwise direction, which results in regulating the flow of extracellular fluid in the leftward direction. This fluid flow is required for establishing the left-right axis and disruption of cilia present on the embryonic node results in *situs inversus* (Nonaka et al., 1998).

In addition ciliopathies have been implicated in causing several disorders and syndromes. Bardet-Biedl syndrome (BBS) patients display pleiotropic symptoms including obesity, retinal dystrophy, *situs inversus*, mental retardation and polydactyly (Tobin & Beales, 2007). Until date, 12 *bbs* genes have been identified and most of these BBS proteins have been shown to localize to the cilia (Badano et al., 2003, Mykytyn et al., 2001). More importantly, they are required for the formation of these organelles. In order to understand the cause of the phenotypes observed in BBS patients, focus has shifted to other proteins that also localize to the cilia. Thus far, two G protein coupled receptors, somatostatin receptor 3 (Sstr3) and melanin concentrating hormone receptor 1 (Mchr1) localize to the cilia (Berbari et al., 2008). Sstr3 is a receptor for somatostatin, a neuropeptide hormone that affects neurotransmission and is considered as a potential factor responsible for mental retardation in BBS patients (Handel et al., 1999). Mchr1 is

important for regulating feeding behavior and is an ideal candidate for understanding obesity related to the syndrome (Pissios, Bradley & Maratos-Flier, 2006). Ciliary localization of such molecules that can be specifically related to specific symptoms is additional evidence that defects in cilia result in many disorders.

Subsequently, components of the IFT machinery that are clearly required for the formation or maintenance of cilia have become targets for intense investigation in order to further understand ciliopathies and other syndromes (Krock & Perkins, 2008, Pazour et al., 2000, Sun et al., 2004). A fine example of how defective IFT protein can be linked to ciliopathies was uncovered in the $Tg737^{orpk}$ mutant mouse. $Tg737^{orpk}$, a hypomorphic allele of IFT88 gene in mice, develop cystic lesions in the kidney similar to that observed in PKD patients. Additionally, these mutants form normal photoreceptors initially but are unable to maintain them, resulting in gradual photoreceptor degeneration (Pazour et al., 2002a). Based on clinical studies, a recessive mutation in IFT80 is associated with Jeune asphyxiating thoracic dystrophy (JATD). Knockdown of IFT80 in zebrafish resulted in kidney cyst accompanied with pericardial edema (Beales et al., 2007). In conclusion retinal degeneration, obesity, kidney cysts, hydrocephaly and left-right asymmetry are characteristic phenotypes caused by compromised ciliary function. Also, several human syndromes mentioned earlier display different combinations of these phenotypes, strongly implicating a role for cilia and thereby IFT in these syndromes (Beales et al., 2007, Pazour et al., 2002b).

1.12. Research aims and significance

Vision loss due to defects in the lens, cornea, retina and other layers occurs in approximately 68% of the western population (Gross & Perkins, 2008). Specifically, retinal degeneration has been observed in Bardet-Biedl syndrome, Jeunes asphyxiating syndrome and retinitis pigmentosa. Hence, understanding the basic cell biology and molecular mechanisms of the photoreceptor layer can aid in development of potential retinal therapies.

The connecting cilium is now a well established structure that is critical for photoreceptor outer segment maintenance and formation. Components trafficked to the photoreceptor outer segment are mislocalized when the connecting cilium is disrupted. It is hypothesized that this mislocalization could be a potential cause for degeneration that is observed in the retina. For instance, the C-terminal region of rhodopin is critical for its normal transport to the OS (Perkins, Kainz, O'Malley & Dowling, 2002, Tam, Moritz, Hurd & Papermaster, 2000). Mutations in rhodopsin result in accumulation of the protein in the inner segment region, leading to photoreceptor degeneration (Chen et al., 2006). Coincidentally, studies in humans also implicate the requirement of rhodopsin for normal functioning and maintenance of photoreceptors (Sung et al., 1991). These data show that retinal degeneration can result from a defect in either the photopigment molecules themselves or the machinery required to transport them. Consequently, components of the IFT machinery serve as ideal candidates to further our knowledge on human blindness.

This project focuses on three specific IFT subunits, IFT57, IFT88 and IFT172, that have been shown to have profound effects on the retina (Gross et al., 2005, Krock & Perkins, 2008, Tsujikawa & Malicki, 2004). Work from our lab previously found that IFT57 mutant zebrafish had short outer segments, whereas IFT88 and IFT172 mutants completely lack outer segments at 5 days post fertilization (dpf) (Gross et al., 2005, Krock & Perkins, 2008). *oval* mutants form sensory cilia but are unable to maintain them, resulting in lack of outer segment formation (Tsujikawa & Malicki, 2004).

The long-term survival of photoreceptors in IFT57, IFT88 and IFT172 mutants have been investigated, however, their effects on early developmental morphogenesis remains poorly understood. To understand this, we analyzed the three IFT mutants at 60 hpf, 72 hpf, and 96 hpf (hours post fertilization), by transmission electron microscopy and immunohistochemistry to chart the progress of photoreceptor morphogenesis and examine the distribution of proteins destined for the outer segment. My specific aims were as follows:

1) To provide an in depth ultrastructural description of outer segment formation in all three mutants, IFT57, IFT88 and IFT172 at three specific time points.

2) To measure outer segment length in the mutants and wild type at each time point. This will allow us to statistically compare and understand whether outer segments in these mutants form and degenerate or if they never form at all.

3) Analyze photoreceptor morphology and the localization pattern of components that are a part of the IFT machinery at the same time points.

1.13. Zebrafish as a model organism

For this project, zebrafish was chosen as it offers several advantages over other established model systems, such as *Drosophila* and mice. Zebrafish is a fresh water teleost that is gaining popularity as a model system for understanding eye development in vertebrates. The zebrafish retina is very similar to that of humans with respect to development and organization (Gross & Perkins, 2008). The anatomy and differentiation pattern of zebrafish retina has been studied extensively and is well documented (Schmitt & Dowling, 1994, Schmitt & Dowling, 1996). Moreover, visual development is rapid, with the first postmitotic neuron forming at 28 hpf followed by differentiation of cells into the various retinal layers forming a functional eye by 72 hpf (Easter & Nicola, 1996, Hu & Easter, 1999). Zebrafish possess a cone-dense retina which helps in understanding cone degenerations as opposed to rod dominant mice. In contrast to mice, zebrafish embryos are born ex-utero and transparent, allowing observation of internal anatomy from the one cell stage.

Other characteristics that have made it an attractive model are its high fecundity wherein it can produce at least 100-200 embryos from a single pair cross, cost effectiveness and easy maintenance. Genetic manipulations are comparatively easy in zebrafish and several mutagenesis screens have helped isolate thousands of mutations affecting zebrafish development (Driever et al., 1996, Haffter & Nusslein-Volhard, 1996). Even though *Drosophila* possesses similar advantages of a short life cycle, tractable genetics and large number of offspring, they differ in certain critical aspects from the vertebrate eye. Invertebrates possess a compound eye and vision occurs by

depolarization of photoreceptors as opposed to the simple eye and hyperpolarization observed in vertebrates. Moreover, the morphology of photoreceptors in flies differs from those observed in vertebrates (Goldsmith & Harris, 2003). Taking all of this into consideration, zebrafish serves as an ideal model system to study the vertebrate retina.

2. MATERIALS AND METHODS

2.1. Zebrafish care and maintenance

The zebrafish *oval* locus encodes IFT88 and *oval* mutants contain a nonsense mutation resulting in a premature stop codon identified in exon 11 (Tsujikawa and Malicki, 2004). The IFT88 null mutant zebrafish were a gift from Jarema Malicki. IFT57 and IFT172 mutants were obtained from a retroviral insertional mutagenesis screen (Gross et al., 2005). All fish were maintained in accordance with established procedures (Westerfield, 1995).

2.2. Transmission electron microscopy

All mutants and wild type fish were fixed at 60 hpf, 72 hpf and 96 hpf in 1% paraformaldehyde, 2.5% glutaraldehyde and 1% tannic acid at 4ºC for 1.5 hours. Embryos were then washed twice in rinse buffer (3% sucrose, 0.15M calcium chloride, 0.06M sodium phosphate buffer). Embryos were processed with osmium tetroxide as secondary fixative for 1.5 hours at 4ºC followed by two washes in rinse buffer. Embryos were dehydrated in water-ethanol series (10% through 100% in increments of 10%) for 10 minutes each. This was followed by washing the embryos twice with a transitional solvent, propylene oxide, for 15 minutes each. Embryos were infiltrated with a graded epoxy resin series (25:75, 50:50, 75:25 and 100% resin to propylene oxide) as previously described (Krock & Perkins, 2008). Transverse sections (0.1 μm in thickness) obtained at the optic nerve region were post-stained with 2% uranyl acetate

and Reynolds lead citrate. Images were acquired with a JEOL 1200EX transmission electron microscope and processed with Adobe Photoshop.

2.3. Immunohistochemistry

Embryos at the designated time points were fixed overnight in 4% paraformaldehyde at 4ºC. Fixed embryos were then washed in PBS three times for 10 minutes each and then placed in 30% sucrose until embryos sunk to the bottom of the tube as described previously (Perkins et al., 2005). They were then embedded in Tissue Freezing medium used for frozen tissue specimens. Frozen molds with embedded embryos were sectioned in a cryostat at -20ºC. 10 μm sections were placed on gelatin coated glass slides. The sections were allowed to dry onto the slide and outlined with a hydrophobic PAP pen and rehydrated in PBST for 15 minutes. Sections were blocked (5% normal goat serum, 1% DMSO) for one hour at room temperature and then incubated in appropriate antibodies overnight at 4ºC. Slides were fluorescently labeled with anti-mouse and anti-rabbit secondary antibodies diluted at 1:500 (Invitrogen) for one hour in the dark at room temperature. Finally, slides were washed in PBST three times for 10 minutes each and mounted with Prolong Gold (Invitrogen P36930). DAPI (1:400) was used as a counter stain. The dilution of primary antibodies used were as follows: monoclonal 1D1 (1:100), monoclonal ZPR1 (1:200), monoclonal anti-acetylated tubulin (Sigma 1:500), polyclonal IFT52 (1:3000) and polyclonal IFT88 (1:5000) (Krock & Perkins, 2008). Images were acquired using an AxioImager fitted with an ApoTome attachment (Zeiss) and processed with Adobe Photoshop.

2.4. SDS-PAGE and western blotting

Embryo heads were cut at 60, 72 and 96 hpf in a Petri dish filled with PBS and ice. Lysis buffer (PBS + 1% Triton + 5mM EDTA) was added at 3 µl per head. The lysate was homogenized and sonicated for 2-3 seconds three times while the tube was placed in an ice bucket. The lysate was then diluted in 4X SDS buffer to which β-mercaptoethanol was freshly added. The solution was boiled at 95°C for 5 minutes and centrifuged for 10 minutes at 13,200 rpm. Samples were loaded on 12% Tris-HCl ready gels (Bio-Rad). The gels were run at 100V until the bands of interest separated sufficiently. The gels were used to set up western blots and proteins were then transferred onto a PVDF membrane at 350mA for an hour. The following steps were performed such that the membrane was subjected to mild agitation. The membrane was blocked in 5% non-fat dry milk in TTBS for 2 hours at room temperature. This was followed by incubation with primary antibodies diluted to the appropriate concentration in the blocking solution, overnight at 4 °C. The membrane was washed three times in TTBS (0.5% Tween-20 in Tris buffered saline) for 10 minutes each and incubated in appropriate secondary antibodies (Exacta Cruz anti- mouse B-HRP and Exacta Cruz anti-rabbit F-HRP, Santa Cruz Biotechnology) for two hours at room temperature. Finally, it was washed in TTBS three times for 10 minutes each and one final wash in TBS. Primary antibody dilutions used are as follows: Rabbit anti-IFT88 (1:3000), Rabbit anti-IFT52 (1:1500) and mouse anti-acetylated tubulin (1:10,000) (Sigma). Super Signal West Femto Maximum Sensitivity Substrate (Thermo Scientific) and

Immunostar HRP substrate Kit (Bio-Rad) was used as secondary antibodies for detection of IFT antibodies and acetylated tubulin, respectively.

3. RESULTS

Zebrafish carrying homozygous mutations in the IFT57, IFT88 and IFT172 genes independently, exhibit photoreceptor degeneration (Gross et al., 2005, Krock & Perkins, 2008, Tsujikawa & Malicki, 2004). Previous studies focused on photoreceptor phenotypes at 4-5 dpf, when outer segments were missing or clearly degenerating. It is not clear, however, if outer segment formation ever occurs normally in these mutants, or if the initial stages of morphogenesis also exhibit perturbations. To understand the progress of outer segment morphogenesis and maintenance in zebrafish IFT mutants, we examined outer segment formation at 60 hpf, 72 hpf and 96 hpf. The 60 hpf time point was the earliest time point chosen because the first photoreceptors begin to differentiate at 50-54 hpf (Hu & Easter, 1999) and the first outer segments can be readily observed at 60 hpf (Schmitt & Dowling, 1999). Analyses at 72 and 96 hpf were used to determine defects in outer segment development as retinas matured (Nawrocki, 1985).

3.1. Electron microscopic analysis at 60 hpf

We used transmission electron microscopy to analyze early photoreceptor anatomy and outer segment structure at 60 hpf in all three IFT mutants. Transmission electron microscopic study of wild type photoreceptor architecture at 60 and 72 hpf has been previously described in detail (Schmitt & Dowling, 1999). Consistent with these previous studies, we observed similar features in wild type embryos at 60 hpf, such as large numbers of mitochondria in the inner segments and small outer segments in the ventral patch (Fig. 6A). We found that outer segments were also present in IFT57 mutants at this time point (Fig. 6B). These outer segments contained regularly stacked

disk membranes and did not appear significantly different than wild type. Statistical analyses using Student's t-test between wild-type and IFT57 mutant embryos revealed no difference in outer segment length at this time point ($p>0.05$) (Fig. 10A). In contrast, we never observed organized disk membranes resembling an outer segment in IFT88 or IFT172 mutants (Fig. 6C-D). In wild-type embryos the region beneath the RPE and above the inner segment region is separated by gaps called the interphotoreceptor space (IPS) that has been observed previously at 50 hpf but not at later time points (Schmitt & Dowling, 1999). However, the IPS was present in all three mutants even at 60 hpf (Fig. 7B-D). Interestingly, we occasionally observed disorganized membranous structures in the apical region of the inner segments of IFT172 mutants but connecting cilia were not detected. These disorganized structures did not resemble outer segments and appeared to distort the apical surface of the inner segment (Fig. 6D). Disorganized arrays of membrane as well as normal outer segments were found in IFT57 mutants (data not shown). These structures were typically located at the apical portion of the cell. On rare occasions, we observed parallel arrays of membrane along the lateral membrane of all IFT mutants, which were similar to the ones observed along the lateral membrane for IFT88 mutants at 88 hpf (Tsujikawa & Malicki, 2004).

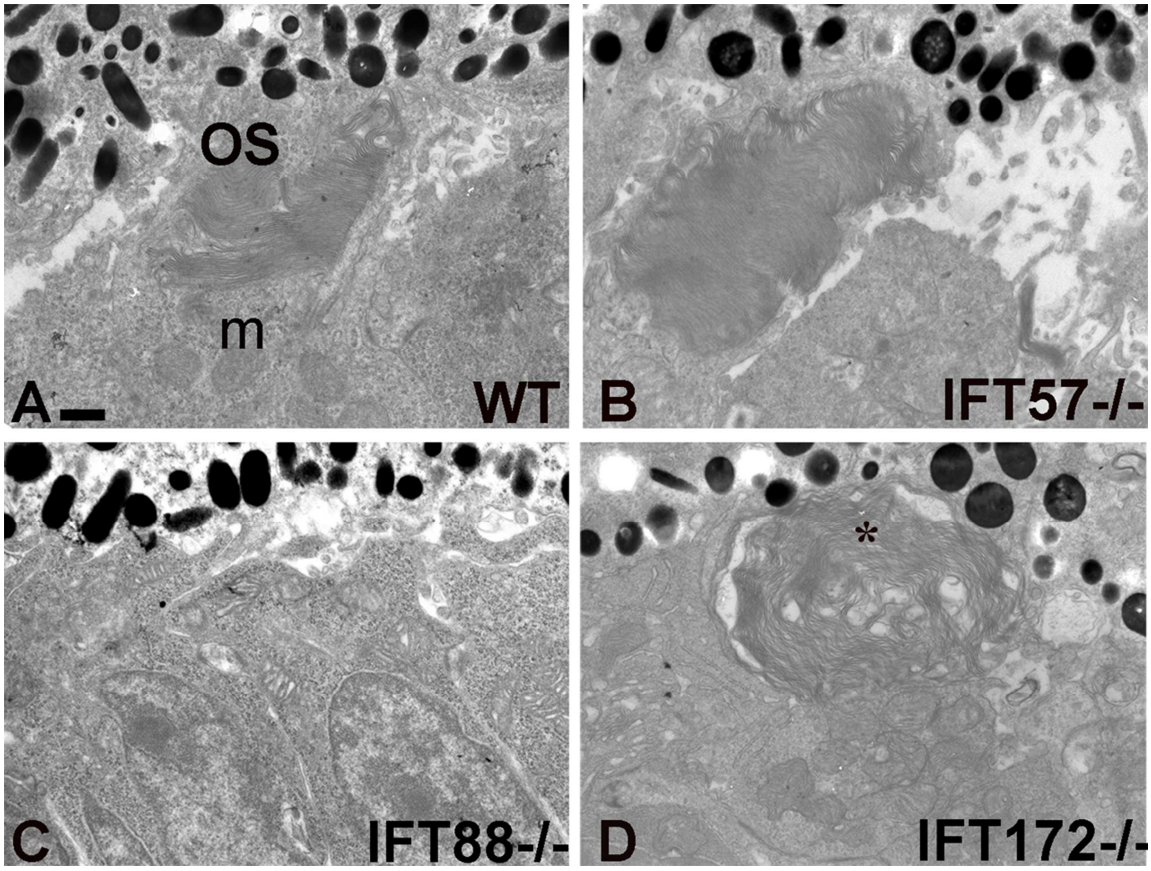

Figure 6. Transmission electron microscopy of wild type, IFT57, IFT88 and IFT172 mutant zebrafish at 60 hpf.

A. Wild-type embryos contained mitochondria (m), and organized stacks of membranes within the outer segment (OS). B. IFT57 mutant embryos also contained photoreceptor outer segments. C-D. No outer segments were observed in IFT88 and IFT172 mutant embryos, although other cellular structures appeared normal. Asterisk in D highlights disorganized membranous structures identified IFT172 mutants. Similar loosely disorganized stacks were observed in IFT57 and IFT88 mutants. Scale bar = 500nm.

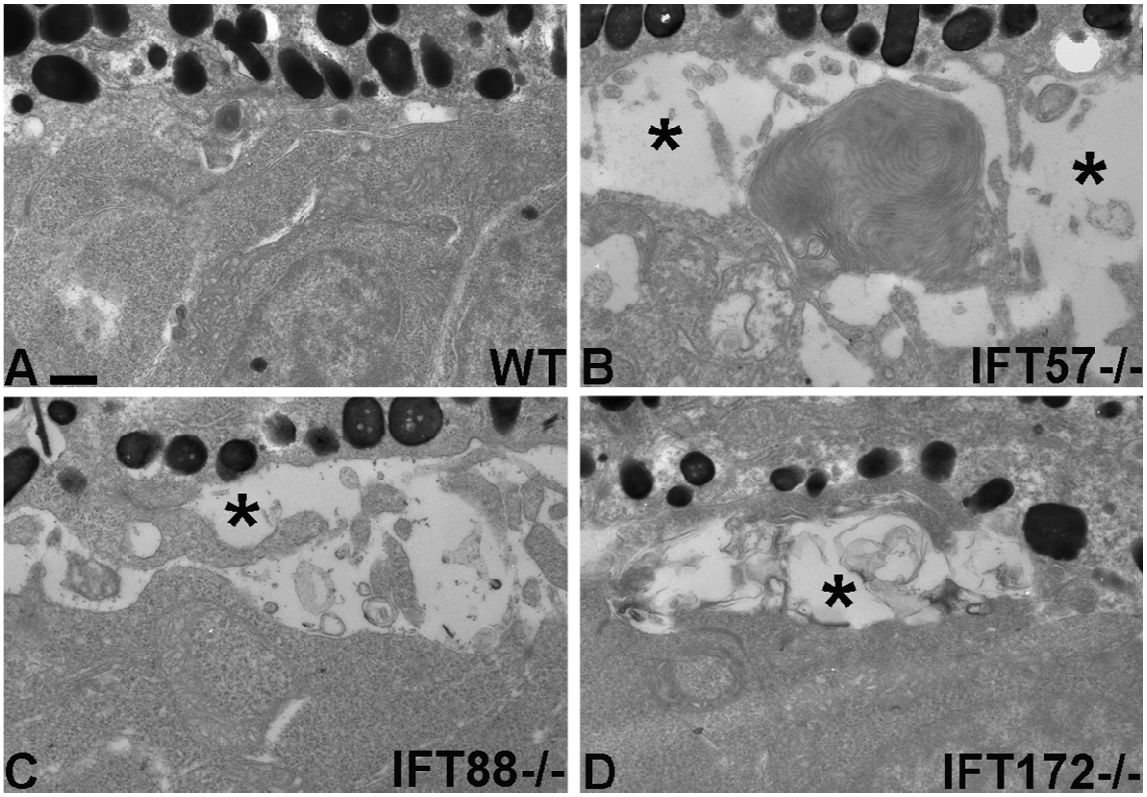

Figure 7. Interphotoreceptor space observed in IFT57, IFT88 and IFT172 mutant zebrafish at 60 hpf.

A. The interphotoreceptor space is not present in the region beneath the RPE in wildtype. B-D. All three mutants show presence of IPS with presence of particulate matter in this space as indicated by the asterisks. Scale bar = 500nm.

3.2. Electron microscopic analysis at 72 hpf

We next examined the IFT mutants at 72 hpf to investigate elongation of outer segments and further photoreceptor differentiation. As described previously, wild-type larvae at 72 hpf showed an increase in the number of outer segments from the previous time point and an increase in width of the inner plexiform layer. Also, small lipid droplets were present in the RPE as the RPE begins to intercalate with the outer segments (Schmitt & Dowling, 1999). Surprisingly, we did not observe an increase in outer segment length between 60 hpf and 72 hpf. At 72 hpf, a small number of outer segments were still observed in IFT57 mutants (Fig. 8B), but the number was reduced by 88% when compared to the wild type (Fig. 10B). However, the existing outer segments showed no difference in length from the wild type ($p>0.05$) (Fig. 10C). Outer segments were still absent in IFT88 and IFT172 mutant embryos at this time point, suggesting that outer segment formation and ciliogenesis failed to occur and was not simply delayed (Fig. 8C-D). We continued to observe disorganized membranous structures in the IFT172 mutants, although these membranes appeared more degenerative than at 60 hpf (Fig. 8D).

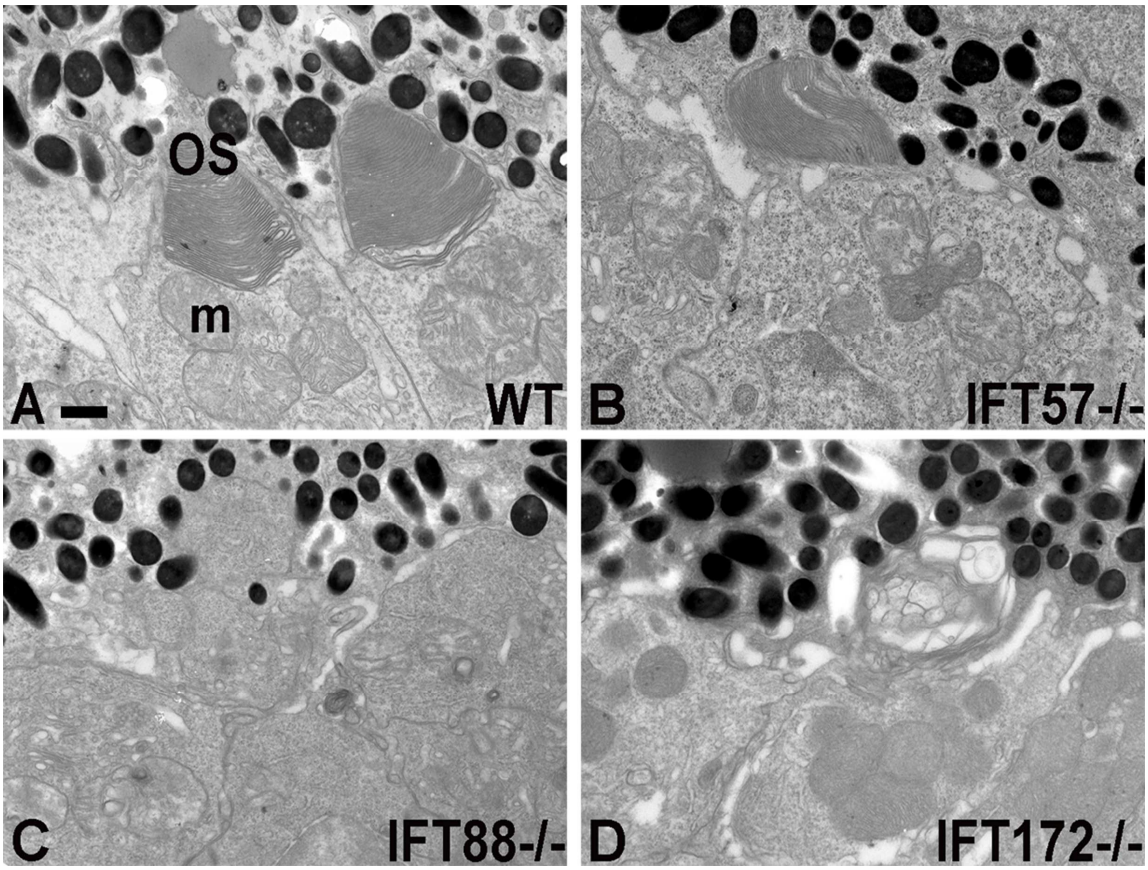

Figure 8. Transmission electron microscopy of wild type, IFT57, IFT88 and IFT172 mutant zebrafish at 72 hpf.

A. Wild-type embryos contained mitochondria (m), and tightly stacked disc membranes within the outer segment (OS). B. IFT57 mutants also contained outer segments.

C-D. Outer segments were absent in IFT88 and IFT172 mutants. Disorganized membranous structures were seen in the apical region of IFT172 mutants. Scale bar = 500nm.

3.3. Electron microscopic analysis at 96 hpf

At 96 hpf, the outer segments of both rod and cone photoreceptors can be observed throughout the retina and photoreceptor nuclei begin to exhibit tiering within the outer nuclear layer (Schmitt & Dowling, 1999). As expected from data at 60 and 72 hpf, we did not observe any outer segments in IFT88 and IFT172 mutants (Fig. 9C-D). At 96 hpf, the number of outer segments observed in IFT57 mutants was reduced by 90% when compared to wild type larvae (Fig. 9B & 10D) and pyknotic nuclei and acellular holes were observed by light microscopy, indicating cell death (Krock and Perkins, 2008; and data not shown). In wild type larvae, outer segment length increased significantly between 72 hpf and 96 hpf to almost 4 microns (Fig. 9A & 10E). In contrast, outer segments in IFT57 mutants did not increase in length when compared to the earlier time points. However, their length was reduced by 38% relative to the wild type (Fig. 10E). These data indicate that IFT57 mutant photoreceptors were unable to grow significantly and maintain the outer segment length like wild type animals.

We previously noted that IFT57 mutant photoreceptors were 75% shorter at 96 hpf (Krock and Perkins, 2008). In the previous work, however, outer segment measurements were limited to the ventral retina where photoreceptor differentiation initiates and where the oldest, and therefore largest, photoreceptors reside. In our current analysis, we measured outer segments from both rods and cones throughout the entire retina and included measurements of outer segments from younger photoreceptors in both wild type and IFT57 mutants. Thus, IFT57 mutant photoreceptors remain shorter than wild type, but ventral photoreceptor outer segments were much shorter than wild type relative to dorsal photoreceptors. Even at this late stage of development, we failed to observe any outer segments in IFT88 and IFT172 mutant embryos (Fig. 9C-D). Disorganized membranous structures were found at all time points in the three mutants. The loosely arranged stacks possibly represent membranous material that failed to extend apically and form outer segments, thus leading to degeneration of photoreceptors in the mutants. Collectively, these data draw a picture of failed attempts at outer segment morphogenesis in IFT88 and IFT172 mutants and the inability to maintain outer segments in IFT57 mutants, all of which result in maturation defects and ultimately premature cell death.

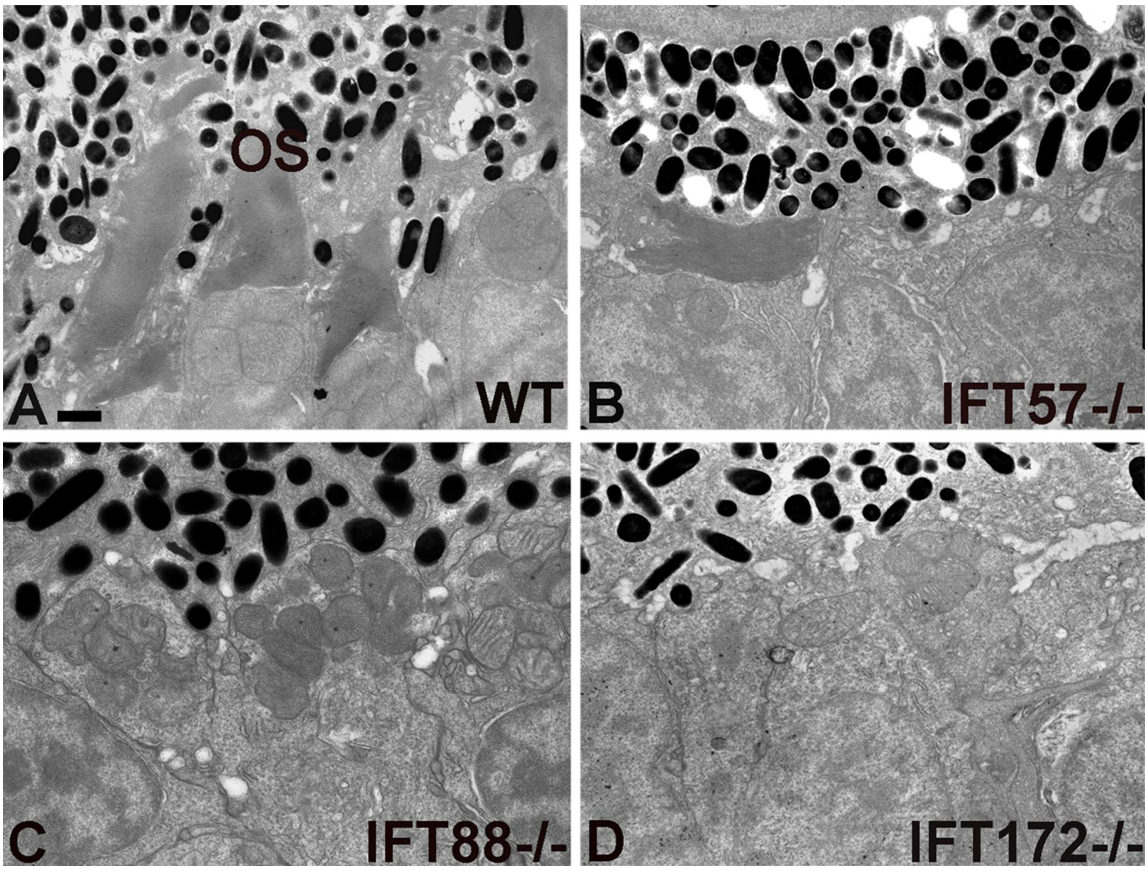

Figure 9. Transmission electron microscopy wild type, IFT57, IFT88 and IFT172 mutant zebrafish at 96 hpf.

A. High magnification images revealed longer outer segments in wild type embryos.

B. Photoreceptor outer segments were present in IFT57 mutants but were shorter than wild type. Mitochondria, nuclei appear to be normal in the mutants. C-D. No outer segments were present in IFT88 and IFT172 mutants. Scale bar = 500nm.

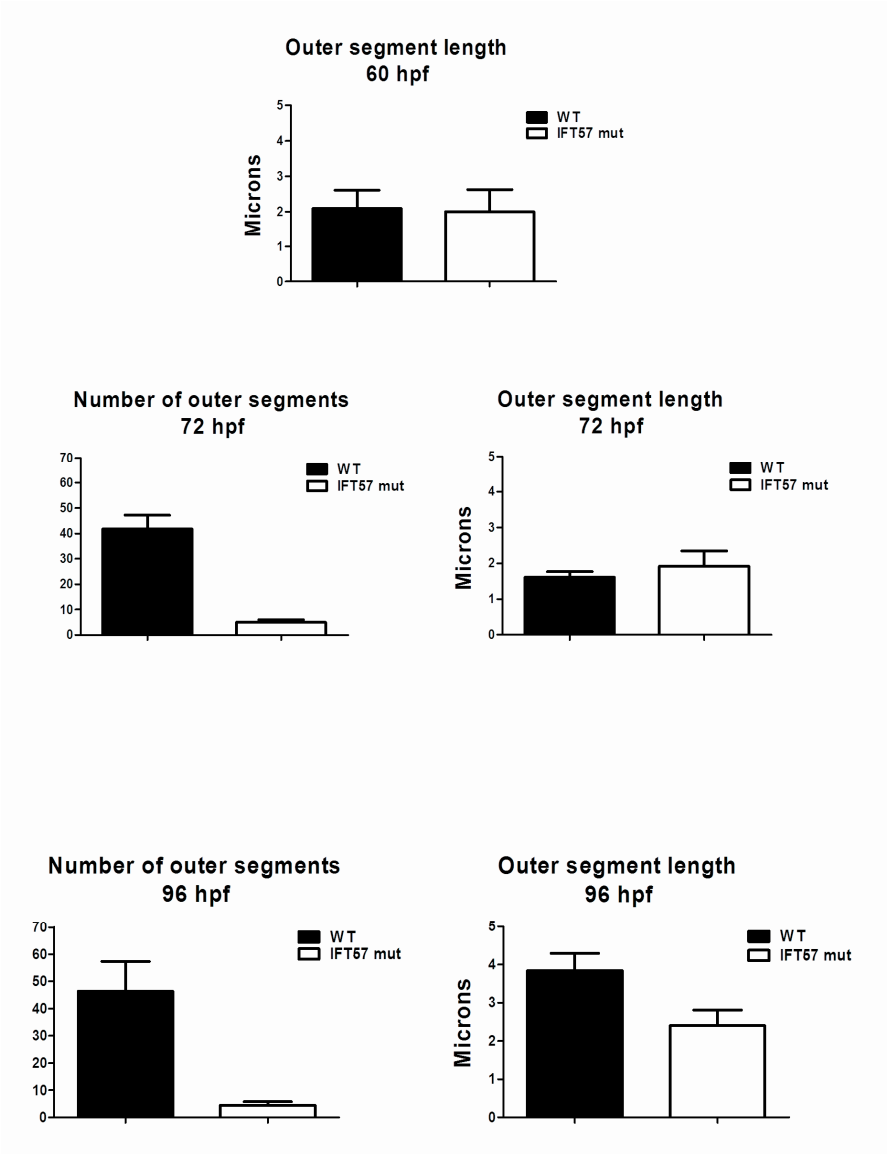

Figure 10. Statistical analysis comparing the number and length of outer segments between wild type and IFT57 mutants.

A. At 60 hpf, IFT57 mutants showed no difference in length when compared to wild types. B-C. At 72 hpf, the number of outer segments (OS) in IFT57 mutant zebrafish was reduced by 88% with no difference in outer segment length. D-E. At 96 hpf, the number and length of outer segments was reduced by 90% and 38% respectively.

3.4. Immunohistochemical analysis at 60 hpf

To complement the TEM data, we performed immunohistochemistry to identify defects in protein trafficking and cell morphology. We first used zpr1, which is also known as Fret-43 and stains red/green double cones, to investigate cell morphology of cone photoreceptors. Zpr1 was seen in the ventral patch in both wild types and mutants at 60 hpf (Fig. 11A-D). This was expected, since the first photoreceptors exit mitosis and differentiate in the ventral patch (Hu & Easter, 1999) and cones migrate dorsally from both the nasal and temporal sides of the retina (Schmitt & Dowling, 1996). Normal cone morphology, as noted by the columnar shape and even distribution of the cells, was observed in wild type sections, as well as all three IFT mutants. Lack of outer segments in the mutants led us to hypothesize that rhodopsin, a protein that is normally localized to the outer segment might be mislocalized to the inner segment in the mutants. We stained retinal sections of 60 hpf embryos using 1D1, an antibody against rhodopsin. While rhodopsin mRNA can be observed as early as 50 hpf in wild type embryos (Schmitt & Dowling, 1996), only a limited number of cells were observed with rhodopsin immunoreactivity. The cells that were positive for rhodopsin revealed normal rhodopsin localization to the outer segment in both wild type and IFT57 mutants (Fig. 11E-F). In contrast, both IFT88 and IFT172 mutants exhibited rhodopsin mislocalization to the inner segment and plasma membrane, indicating that protein trafficking was abnormal in these mutants (Fig. 11G-H). As the formation of outer segments requires extension of a primitive cilium, we confirmed the presence of cilia by using an antibody against acetylated tubulin. Cilia were observed in both wild type and

IFT57 mutants, which was expected as outer segments were seen in IFT57 mutants by transmission electron microscopy (Fig. 11I-J). Consistent with our TEM data, we failed to detect acetylated tubulin staining in IFT88 and IFT172 mutants, which further supports the conclusion that ciliary structures do not form in these mutants (Fig. 11K-L). We next investigated whether loss of individual IFT components affected the localization of other IFT proteins. We used antibodies against IFT52 and IFT88 (Krock & Perkins, 2008) to examine IFT particle localization. At 60 hpf, we observed immunoreactivity against both proteins in wild type sections but not in any of the mutants (Fig. 11M-T). This led us to propose two possibilities; 1) The IFT52 and IFT88 subunits were absent in the mutants or 2) Loss of other IFT components resulted in mislocalization of IFT52 and IFT88 protein and redistribution throughout the cell such that the concentration of these polypeptides was below the level of detection by immunohistochemistry. Western blot analysis showed that IFT52 was present in all mutants, although at lower levels than observed in wild type embryos (Fig. 12). IFT88 was present in IFT57 and IFT172 mutants (Fig. 12). We did not detect any IFT88 protein in the IFT88 mutants, consistent with previous studies indicating the *oval* mutants resulted from a null allele (Krock & Perkins, 2008, Tsujikawa & Malicki, 2004).

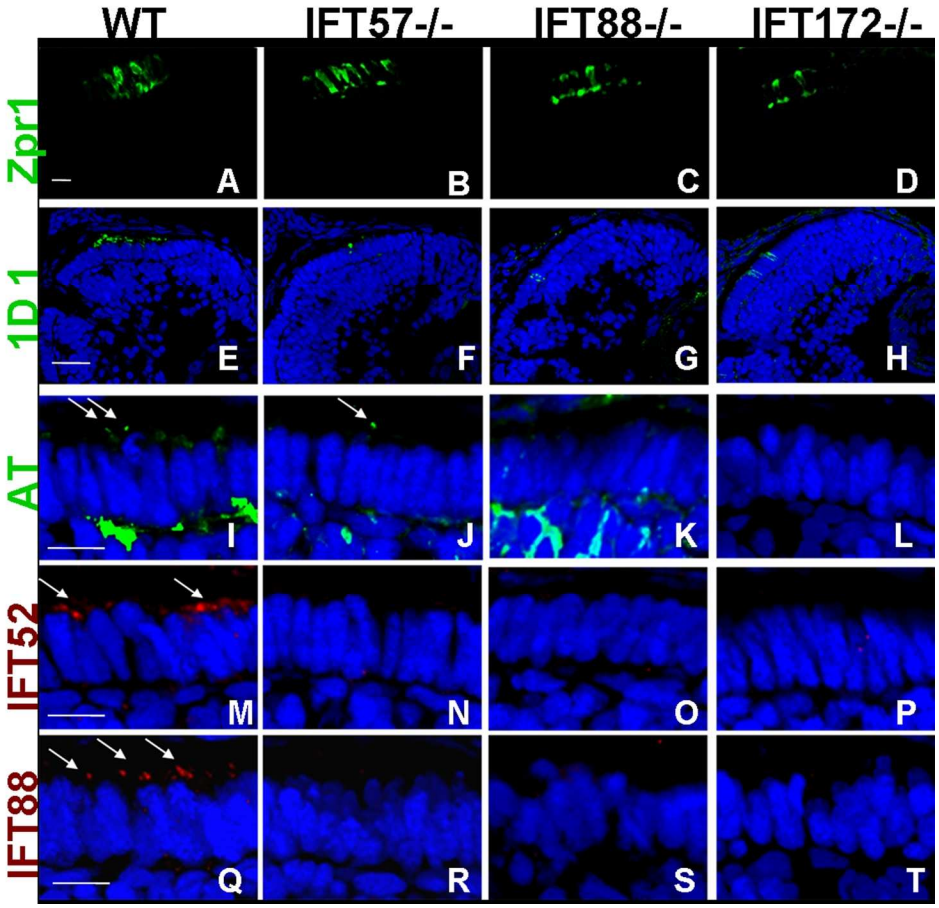

Figure 11. Immunohistochemical analysis of wild type, IFT57, IFT88 and IFT172 mutant zebrafish at 60 hpf.

Scale bar = 20 μm (A-H), 10 μm (I-T).

A-D. Zpr1 (green), a label for red/green double cones, showed normal morphology of these cells in the wild type and mutants. E-F. 1D1 (green), marker for rhodopsin, localized to the outer segment region in wild type and IFT57 mutant retinas. G-H. 1D1 (green) was mislocalized towards the inner segment in IFT88 and IFT172 mutants. I-J. Connecting cilia (arrows) were labeled with acetylated tubulin (green) in both wild type and IFT57 mutants. K-L. Acetylated tubulin (green) was not seen in IFT88 and IFT172

mutants. M. Antibody against IFT52 (red) was seen above the inner segment region (arrows) in wild type. N-P. No label against IFT52 was detected in all three mutants. Q. Antibody against IFT88 (red) also localized to the apical end of the inner segment (arrows) in wild type. R-T. IFT88 immunoreactivity was absent in all three mutants. In all the images (excluding A-D), DAPI (blue) was used as counterstain and labels the nucleus.

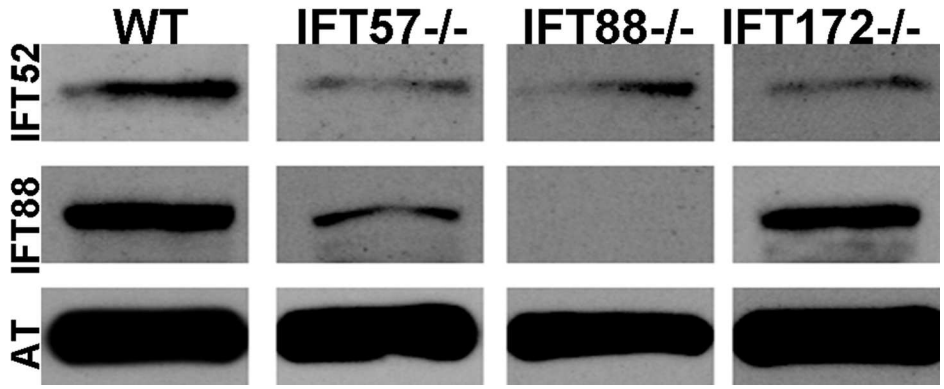

Figure 12. Western blot analysis at 60 hpf.

Antibody against IFT52 was detected in wild type, IFT57, IFT88 and IFT172 mutants. Antibody against IFT88 was present only in the wild type, IFT57 and IFT172 mutants, showing that the IFT88 mutant was null. Acetylated tubulin (AT) served as a control.

3.5. Immunohistochemical analysis at 72 hpf

Changes in photoreceptor health were first evident by 72 hpf and became more pronounced by 96 hpf. Staining with zpr1 revealed that the cone morphology remained normal in all three mutants (Fig. 13A-D) and is consistent with previous studies on

IFT88 mutants (Doerre and Malicki, 2002). By 72 hpf, more cells exhibited rhodopsin localization in the outer segments of wild type embryos (Fig. 13E). In contrast, rhodopsin found in both the outer and inner segment region of IFT57 mutants, indicating that protein trafficking was disrupted in these mutants (Fig. 13F). IFT88 and IFT172 mutant embryos showed complete mislocalization of rhodopsin, consistent with the lack of outer segments observed with TEM (Fig. 13G-H). Antibodies against acetylated tubulin revealed the presence of connecting cilia in wild type and IFT57 mutants, (Fig. 13I-J) but not in the IFT88 and IFT172 mutants (Fig. 13K-L). This was further evidence that initiation of outer segment morphogenesis requires IFT88 and IFT172. Antibodies against IFT52 and IFT88 localized to the basal body region and connecting cilia in the wild type (Fig. 13M, Q). However, we could still not detect these IFT components in any of the IFT mutants at 72 hpf (Fig. 13N-P & R-T). We performed western blotting at 72 hpf and revealed the presence of IFT52 protein in all three mutants and IFT88 protein in IFT57 and IFT172 mutants (Fig. 14). This data demonstrates that IFT52 and IFT88 were present in the mutants but were likely mislocalized and not detected as previously mentioned. As protein extracts were obtained from embryo heads rather than isolated retinas, we cannot rule out the possibility that IFT proteins are indeed missing from photoreceptors and the immunoreactivity we observed by Western blotting reflects expression in other cell types within the CNS. This seems unlikely, as we observed IFT52 and IFT88 immunoreactivity in the IFT57 mutant photoreceptors at later time points when photoreceptors were more mature (see below).

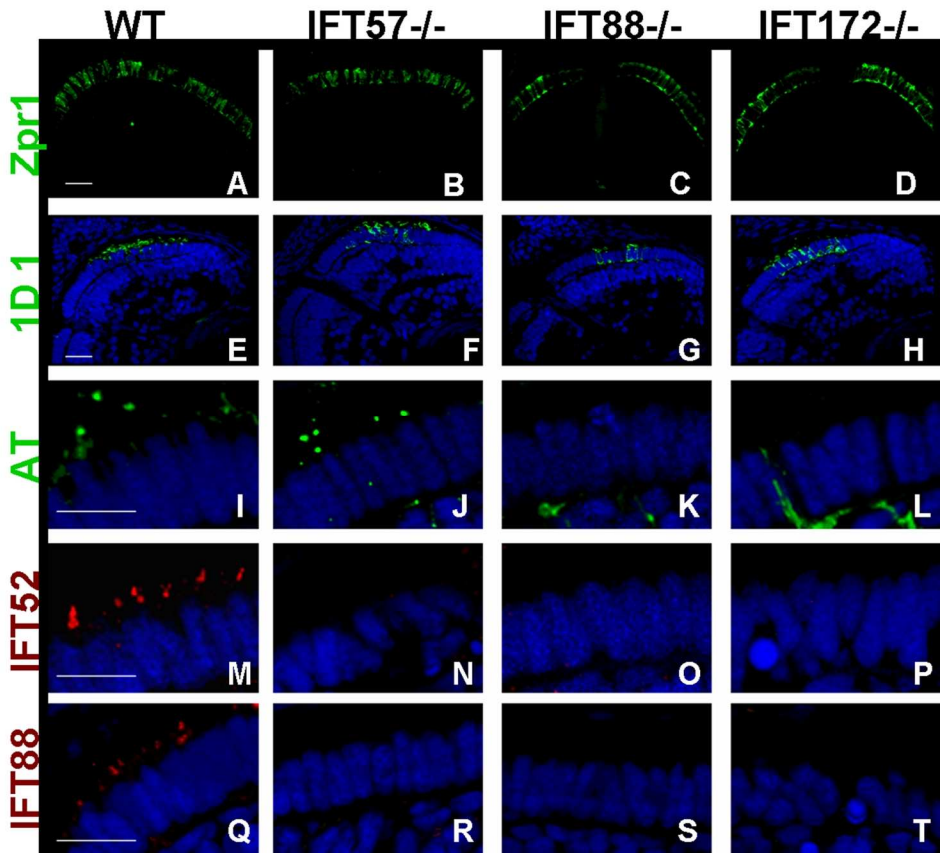

Figure 13. Immunohistochemical analysis of wild type, IFT57, IFT88 and IFT172 mutant zebrafish at 72 hpf.

Scale bar = 20 μm (A-H), 10 μm (I-T).

A-D. Zpr1 (green), label for red/green double cones showed presence of healthy, columnar shaped cells in wild type and mutants. E. 1D1 (green), marker for rhodopsin, localized to the outer segment region in wild type. F. 1D1 (green) was present in outer segment region in IFT57 mutant, however there was some mislocalization towards the inner segment also. G-H. 1D1 (green) was mislocalized towards the inner segment in IFT88 and IFT172 mutants. I-J. Connecting cilia labeled with acetylated tubulin (green)

was seen as punctuate dots above the inner segment region in wild type and IFT57 mutants. K-L. Acetylated tubulin (green) immunoreactivity was not observed in IFT88 and IFT172 mutants. M. Antibody against IFT52 (red) was seen in basal bodies and connecting cilia in wild type. N-P. No label against IFT52 was detected in all three mutants. Q. Antibody against IFT88 showed similar labeling pattern as IFT52 in wild type. R-T. No IFT88 immunoreactivity was seen in all the mutants. E-T. DAPI (blue) was used as a counter stain that labeled the nucleus.

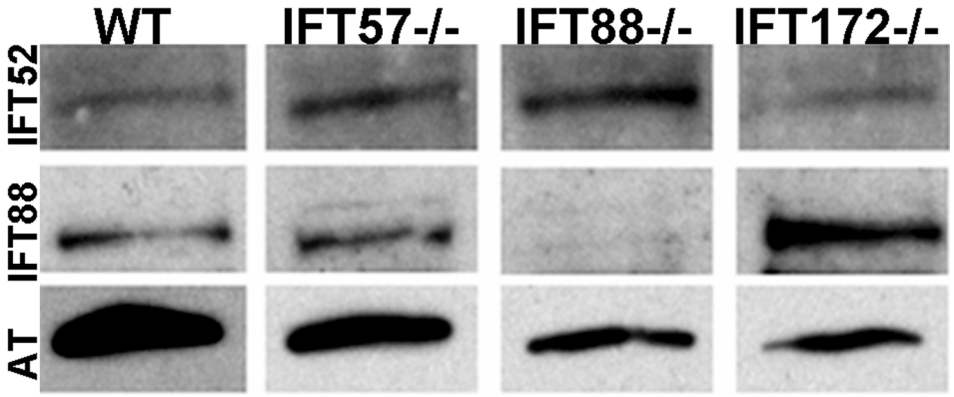

Figure 14. Western blot analysis at 72 hpf.

Antibodies against IFT52 and IFT88 were detected in wild type and mutants at 72 hpf, confirming the expression of these subunits. IFT88, as expected, was not seen in the IFT88 mutant as it was null but continued to be expressed in other mutants as well as wild type. Acetylated tubulin (AT) served as a control.

3.6. Immunohistochemical analysis at 96 hpf

Immunohistochemistry analysis at 96 hpf revealed more dramatic changes in photoreceptor structure and protein localization. Zpr1 labeling at 96 hpf showed that the mutant cone photoreceptors acquired a disheveled appearance, suggestive of degeneration due to the lack of outer segments (Fig. 15A-D). Staining with 1D1 revealed that rhodopsin remained mislocalized to the inner segment region in IFT88 and IFT172 mutants (Fig. 15G-H). In IFT57 mutants, rhodopsin was mislocalized more to the inner segment region when compared to the earlier time points (Fig. 15F). This data, along with TEM, supports the idea that IFT57 mutants were unable to maintain outer segments during later development. Staining with acetylated tubulin permitted observation of connecting cilia in the wild type and the remaining photoreceptors in the IFT57 mutants (Fig. 15I-J). Compared to wild type siblings, the number of cilia were significantly reduced in IFT57 mutants, which was consistent with the ultrastructural data showing reduced number of outer segments in this mutant. IFT88 and IFT172 mutants did not show any acetylated tubulin staining in the area predicted for connecting cilia, strongly suggesting that cilia were absent in these mutants (Fig. 15K-L). Staining with antibodies against IFT52 and IFT88 was found localized to the basal body region and connecting cilia in wild type and IFT57 mutants (Fig. 15M, N, Q, R). These IFT components were not detected in IFT88 and IFT172 mutant zebrafish (Fig. 15O, P, S, T). However, western blots from the earlier time points showed that these proteins were expressed in the mutants but could not be detected by immunohistochemistry.

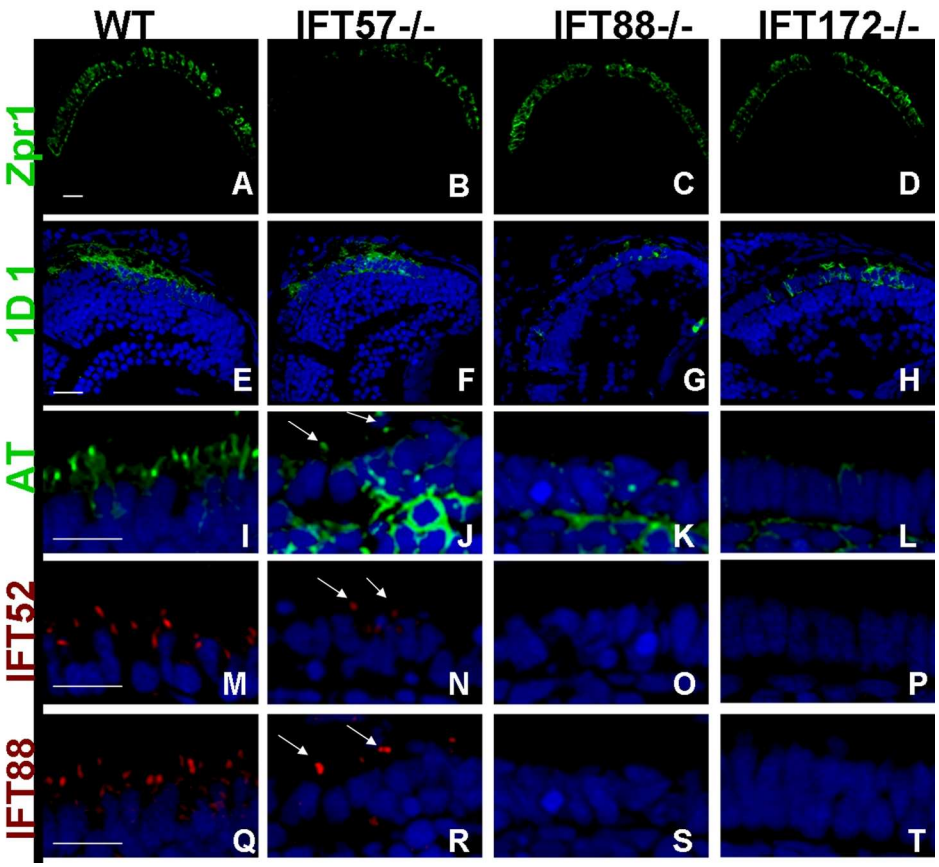

Figure 15. Immunohistochemistry analysis in wild type, IFT57, IFT88 and IFT172 mutant zebrafish at 96 hpf.

Scale bar = 20 μm (A-H), 10 μm (I-T).

A. Zpr1 (green), label for red/green double cones showed normal morphology in wild type. B-D. Morphology of cones was disheveled in the three mutants showing signs of cell death. E. 1D1 (green), marker for rhodopsin, localized to the outer segment region in wild type. F. 1D1 (green) was present in outer and inner segment region in IFT57 mutant. G-H. 1D1 (green) was mislocalized towards the inner segment in IFT88 and IFT172 mutants. I-J. Connecting cilia labeled with acetylated tubulin (green) were present in wild type and IFT57 mutants (arrows in J). K-L. Acetylated tubulin (green)

was not seen in IFT88 and IFT172 mutants. M-N. Antibody against IFT52 was present in wild type and IFT57 mutant (arrows in N). O-P. No label against IFT52 was detected in IFT88 and IFT172 mutants. Q-R. Antibody against IFT88 was present in wild type and IFT57 mutant (arrows). S-T. No IFT88 antibody was seen in IFT88 and IFT172 mutants. In images E-T, the nuclei were labeled with DAPI (blue).

4. DISCUSSION

In this study, we investigated the progression of early photoreceptor morphogenesis in three IFT mutant zebrafish (IFT57, IFT88 and IFT172). A unique aspect of our study was the examination of mutant photoreceptors at 60 hpf when outer segment morphogenesis first becomes apparent in zebrafish (Schmitt & Dowling, 1999). Previous reports focused largely on photoreceptor survival at 4-5 dpf, however, none have reported ultrastructural data as early as 60 hpf. Classic ultrastructural studies suggested that outer segment formation in vertebrates could be divided into three stages (De Robertis, 1956b, De Robertis, 1960). First, a primitive cilium extends from the apical surface of the cell. Second, vesicles and primitive "rod sacs" accumulate at the apical end of the primitive cilium. Third, the membranes undergo remodeling and reorientation to form flattened disks. However, with our current data, we propose a fourth stage, wherein the outer segment matures and extends to its mature length. Our data, as well as previous studies, suggest that the fourth stage is as critical as the previous steps, as the inability to increase outer segment length results in photoreceptor cell degeneration. Our new data reveal that IFT57 mutants can successfully complete the first three stages of outer segment morphogenesis but fail to extend beyond a rudimentary length and subsequently die. Furthermore, we could not find evidence that IFT88 and IFT172 mutant photoreceptors were competent to complete the first stage of extending a primitive cilium.

Prior to these morphogenetic changes occurring in the photoreceptor layer, a characteristic feature of the developing retina is the interphotoreceptor space (ips). The

ips is represented by gaps beneath the RPE and above the photoreceptor inner segment. They are more prominent in the ventral patch region where retinal differentiation is most advanced at 50 hpf (Schmitt & Dowling, 1999). Developing outer segments replace these spaces; consequently the ips is rarely observed in the wild type after 50 hpf. Hence, the ips could potentially signify gaps that are formed in order to accommodate and aid the development of the newly forming outer segments. However, at 60 hpf we continued to observe the large ips beneath the RPE in all three mutants (Fig. 7). Moreover, the ips in these mutants contained broken-up, particulate matter that was spread across the space. We speculate that these gaps persist in the mutants because of their delay or failure in forming outer segments at this time point. Interestingly, the ips was reduced and almost absent in all three mutants after 60 hpf, suggesting that the space exists only for a certain time period during which the cell anticipates initiation of outer segment formation.

Defects in photoreceptor outer segment formation at later developmental stages have been extensively documented for IFT88 mutant zebrafish (Doerre & Malicki, 2002, Krock & Perkins, 2008, Tsujikawa & Malicki, 2004). Consistent with these studies, we do not observe cilia at 72 hpf or 96 hpf by either acetylated tubulin staining or ultrastructural analyses. Although cilia and newly forming outer segments were readily observable in wild type embryos, we were unable to detect primitive cilia or loosely aggregated outer segment material in IFT88 mutants at 60 hpf. In addition, we also observe large holes indicative of photoreceptor cell death by 96 hpf. These data argue that loss of IFT88 completely abolishes cilia formation in photoreceptors, which

consequently results in lack of outer segments. Characterization of individual components of the complex has shown that IFT subunits may play different roles in various ciliated tissues within the animal (Gross et al., 2005, Sun et al., 2004, Tsujikawa & Malicki, 2004). Interestingly, IFT88 mutants can form sensory cilia in the otic vesicle and nasal epithelium during embryogenesis as early as 30hpf, although these cilia are not maintained (Tsujikawa & Malicki, 2004). Explaining these results by a contribution of maternal IFT88 protein appeared unlikely as IFT88 protein was not detected at the 2-cell stage by Western blotting. Moreover, our results concur with studies in mice and *C.elegans*, where lack of IFT88 results in absence of cilia. However, as opposed to the complete lack of outer segments that we observe, $Tg737^{orpk}$ mice, which harbor a hypomorphic mutation in IFT88, possess connecting cilia and outer segments. The outer segments formed in these hypomorphs are abnormal wherein they are shorter and the disc membranes are predominantly broken into smaller segments or aligned in parallel with respect to the connecting cilium. Nevertheless, the small amount of IFT88 expressed in these hypomorphic mutant mice is responsible for the connecting cilia and abnormal outer segments observed in this study (Pazour et al., 2002a). These data strongly argue that the initial assembly and formation of vertebrate photoreceptor outer segments requires IFT88, whereas other ciliated sensory neurons in zebrafish may only require IFT88 for maintenance.

Our work provides the first detailed analysis of how loss of IFT172 affects early photoreceptor development. Previous studies demonstrated that zebrafish IFT172 mutants form kidney cysts (Sun et al., 2004) and they lack outer segments at 5 dpf

(Gross et al., 2005). Our data show that loss of IFT172 results in phenotypes that closely resemble, but are distinctive from that of IFT88 mutants. Like the IFT88 mutants, IFT172 mutants lack outer segments at all time points examined and photoreceptors rapidly degenerate. At 60 and 72 hpf, we frequently observed large accumulations of membranous material at the apical end of the inner segments in IFT172 mutants. While these loosely aggregated membranes were also seen in IFT88 mutants, they were more prominent in IFT172 mutants. These membranes resembled disorganized disk membranes but no connecting cilia were ever observed and the membranes remained closely associated with mitochondria in the inner segment. These data suggest that IFT172 mutant photoreceptors attempted to assemble outer segment material but failed to extend a ciliary structure to contain this material.

Finally, our analysis shows that IFT57 mutant zebrafish develop cilia and outer segments, as opposed to the complete lack of this organelle observed in conventional complex B mutants. Our observed phenotype is similar to *Chlamydomonas* IFT57 mutants that are also reported to have short flagella. In contrast, mutation of *che-13*, the *C.elegans* ortholog of IFT57 yields a phenotype similar to *osm-1*, *osm-5* and *osm-6* which are all a part of complex B (Haycraft et al., 2003). Hippi, the IFT57 ortholog in mice, was initially identified in Huntington disease (HD), a neurodegenerative disorder due to its interaction with HIP-1 (htt interacting protein-1). This interaction results in the formation of a pro-apoptotic complex that triggers cell death. Studies in IFT57 knock-out mice, however, show that it is required for nodal cilia formation and Sonic hedgehog signaling (Houde et al., 2006). Analysis from these three mutants itself shows

that even though IFT is a conserved process, the role of individual IFT subunits in cilia formation differs between species.

These data also extended our previous analysis of IFT57 mutant photoreceptors (Krock & Perkins, 2008) and further characterized photoreceptor outer segment morphogenesis beyond 60 hpf (Schmitt & Dowling, 1999). We expected an increase in wild type outer segment length in proportion to the growth of the eye at all time points. However, the photoreceptors at 60 hpf and 72 hpf showed no significant increase in outer segment length in wild type embryos. Vision can be attributed to the dramatic increase in outer segment number observed at 72 hpf, which collectively helps in the functioning of the photoreceptor layer. Moreover, the outer segments grow rapidly in length from 72 hpf to 96 hpf in wild type animals (Fig. 10). We previously reported that IFT57 mutant photoreceptors have shorter outer segments than wild type at 96 hpf (Krock & Perkins, 2008). This phenomenon can have two possible explanations. Either the mutants fail to make a normal ciliary extension from the beginning, resulting in significantly shorter outer segments as compared to wild type animals at all time points considered. Alternatively, outer segments are initially normal, but cannot grow in length as time progresses. Quantification of outer segment lengths revealed no statistical difference between wild type embryos and IFT57 mutants at 60 and 72 hpf (Fig. 10A,C). This supports the latter hypothesis that the extension of outer segments in the IFT57 mutants initially follows a wild type pattern, but the reduced efficiency of the IFT process results in failed outer segment length maintenance.

As IFT mutants possess defective outer segments resulting in retinal degeneration, we previously inquired as whether these mutants are capable of vision. The Optokinetic response assay (OKR), is a well established tool for determining visual behavior, and has been performed previously on IFT57 and IFT172 mutants at 5 dpf (Gross et al., 2005). As expected, this study showed that visual response in IFT57 mutants was normal at 5 dpf, as they form outer segments that begin to deteriorate subsequently from this time point. Surprisingly, IFT172 mutants showed a weak OKR response, even though they lack outer segments (Gross et al., 2005). OKR assays have not been performed in IFT88 mutants. However, based on data presented in this dissertation and from other studies, we predict that these mutants will either follow a similar response as IFT172 or completely lack any visual reflex. The unexpected visual response observed in these mutants can be further confirmed by performing Electroretinograms (ERGs), which help assay for retina function.

In addition to our phenotypic analysis, we wanted to understand the effects of these mutations at a molecular level. Conditional knock-out of KIF3A, a Kinesin II subunit in mice, results in mislocalization of rhodopsin and arrestin to the inner segment region (Marszalek et al., 2000). Interestingly, $Tg737^{orpk}$ mice also show a higher concentration of rhodopsin in the connecting cilium and inner segment when compared to wild-type mice (Pazour et al., 2002a). Hence, one of the well-established consequences of defective IFT machinery is the abnormal trafficking of rhodopsin to the outer segment. IFT88 and IFT172 showed complete mislocalization of rhodopsin at all time points. On the other hand, IFT57 mutant retinas shows normal transport of

rhodopsin that progressively mislocalizes as the outer segments were not maintained. This result also suggests that the interaction of rhodopsin with the IFT complex does not require IFT57.

Loss of individual IFT components can also affect the localization and stability of other IFT proteins. As IFT57 mutants form outer segments, the IFT52 and IFT88 proteins localized at or near the cilium. Both IFT52 and IFT88 could not be detected by immunohistochemistry in IFT88 and IFT172 mutants. Western blot analysis showed that the IFT52 protein was present in all three mutants at all time points studied. IFT88 was present in only in IFT57 and IFT172 mutants and not in IFT88 mutants, confirming that it was a null mutant. These results agree with data from the analysis of IFT mutants in other species. In *Chlamydomonas*, IFT52 localizes to the distal end of basal body transitional fibers (Deane et al., 2001). Similar to our results, the *C.elegans* IFT52 ortholog OSM-6 localized normally in *C.elegans che-13* mutants, which affect IFT57 (Haycraft et al., 2003). Interestingly, whereas we demonstrated normal localization of IFT88 in IFT57 mutant photoreceptors, the worm IFT88 protein, OSM-5, was mislocalized throughout the dendrite and cell body in *che-13* mutants (Haycraft et al., 2003). Furthermore, OSM-5 (IFT88) localized to the apical tip of the transition zone in the OSM-6 (IFT52) and OSM-1 (IFT172) mutants (Haycraft et al., 2001), whereas we could not detect IFT88 protein near the apical region where basal bodies might form in IFT172 mutants. The experiments in *C.elegans* utilized transgenes expressing IFT-GFP fusion proteins, whereas we analyzed immunofluorescence of fixed tissue. The different techniques used to detect IFT protein localization may explain these differing results, as

the sensitivity of the immunolocalization may be potentially lower than that of an IFT-GFP transgene. Alternatively, the order and composition of IFT particle assembly may differ between sensory cilia in worms and vertebrate photoreceptors. Co-immunoprecipitation assays found that the IFT complex can form in IFT57 mutants but it lacks IFT20 (Krock & Perkins, 2008). In *Chlamydomonas*, it has been shown that there is a decrease in IFT57 and an increase in IFT139 in *Chlamydomonas* IFT88 mutants (Pazour et al., 2000). Our western analysis shows that IFT57 was present in IFT88 and IFT172 mutants, like the other IFT proteins that we had blotted for (data not shown).

Comparing our analysis to previous studies, as well as other model systems such as *Chlamydomonas* and *C.elegans,* confirms that IFT88 is absolutely required for cilia formation (Doerre & Malicki, 2002, Krock & Perkins, 2008, Tsujikawa & Malicki, 2004). Our work also shows that IFT172 has a similar role as IFT88 in photoreceptor development. Lastly, IFT57 is not absolutely required for the initiation of cilia and as described previously this subunits contributes towards maintenance and extension of the structure. Hence our work provides novel details about IFT57, IFT88 and IFT172 in early photoreceptor development and shows how different subunits of the IFT particle can play different roles in the same vertebrate tissue.

5. CONCLUSION AND FUTURE DIRECTIONS

In conclusion, we have provided detailed ultrastructural analyses of IFT57, IFT88 and IFT172 mutants at 60 hpf, the earliest time point corresponding to outer segment formation (Schmitt & Dowling, 1999). Electron micrographs obtained at this time point show that only few outer segments are present in the wild type but as time progresses, the number of outer segments increase significantly. However, the mutants do not grow outer segments at the same pace as the wild type. Our analysis has answered one of the basic questions put forth in this project, which was to understand whether outer segments in the mutants develop and then degenerate or if they never form at all. Statistical analysis at progressive time points shows that the connecting cilia and outer segments never form in the photoreceptors of IFT88 and IFT172 mutants. On the other hand, IFT57 mutants maintain the initial length they achieve by 60 hpf across all subsequent time points implying that the IFT57 protein is required for further growth of the structure (Fig. 10).

Our work also aimed at understanding the localization pattern of proteins that would provide information on photoreceptor morphology and formation of the IFT complex. Gradual photoreceptor degeneration is reflected in cone morphology that is initially normal but by 96 hpf the cells begin to deteriorate. Based on immunohistochemistry and western blot results, we can assume that most IFT subunits are expressed in the mutants. Our analysis nevertheless only focused on identifying whether other subunits were present or absent in the mutants. However based on studies in *C.elegans* IFT mutants, wherein the expression levels of other subunits differ, we can

speculate that such a variation might exist in the mutant zebrafish photoreceptors. Pull down assays performed previously in the IFT57 mutant show that even though IFT20 is expressed in the mutant, it is not a part of the IFT complex (Krock & Perkins, 2008). The next step would be to perform similar westerns in IFT88 and IFT172 mutants, which will help quantify the expression levels of other subunits. Also, pull down assays can be performed in order to understand how loss of these proteins affects IFT particle assembly.

Yeast two-hybrid assays between four IFT subunits, IFT20, IFT52, IFT57 and IFT88 and all the three Kinesin subunits led to the identification of a direct physical interaction between Kinesin II and IFT20. Since it has been established that this binding is not required for anterograde transport, the next step would be to identify the putative protein that has been proposed for this link. An essential experiment for this would be to perform yeast two-hybrid assays for all the other IFT subunits that were not a part of the initial study (Baker et al., 2003). From this screen we will at least be able to determine if Kinesin II is linked to the complex through another IFT subunit.

A broader question that still remains a mystery is the make-up of the cargo that is transported to by the IFT complex. There are several previous localization studies, including our data that implicate rhodopsin as a potential cargo molecule. However, there is no information of a direct link between rhodopsin and the IFT complex. An interesting experiment would be to perform a pull down assay and see whether rhodopsin immunoprecipitates with the IFT complex. Furthermore, a yeast two-hybrid analysis using rhodopsin as the bait against all the individual IFT subunits as prey will

help identify which subunit directly binds to the protein. Other cargo molecules like radial spokes, axonemal proteins and transient receptor potential vanilloid (TRPV) membrane proteins have been identified based on co-immunoprecipitation and localization studies. Again, yeast two-hybrid assays can be performed to recognize which specific IFT subunit, form direct links with these cargo molecules.

The Intraflagellar transport mechanism hence continues to be a topic of intense research due to the several unanswered questions and the complexity of this process. Abnormality of the IFT process leads to retinal degeneration, as a result of which they are good candidates for understanding human diseases such as retinitis pigmentosa. Furthermore, simple model systems like zebrafish, have helped in furthering our understanding of IFT during very early stages of retinal morphogenesis (Krock & Perkins, 2008, Tsujikawa & Malicki, 2004). Information gleaned from these zebrafish IFT mutants can be extrapolated to mammalian systems, thereby aiming towards the development of cures for human retinal dystrophies.

REFERENCES

Afzelius, B.A. (2004). Cilia-related diseases. *J Pathol, 204* (4), 470-477.

Amsterdam, A., & Hopkins, N. (1999). Retrovirus-mediated insertional mutagenesis in zebrafish. *Methods Cell Biol., 60*, 87-98.

Anderson, R.E., & Maude, M.B. (1970). Phospholipids of bovine outer segments. *Biochemistry, 9* (18), 3624-3628.

Apfeld, J., & Kenyon, C. (1999). Regulation of lifespan by sensory perception in Caenorhabditis elegans. *Nature, 402* (6763), 804-809.

Badano, J.L., Ansley, S.J., Leitch, C.C., Lewis, R.A., Lupski, J.R., & Katsanis, N. (2003). Identification of a novel Bardet-Biedl syndrome protein, BBS7, that shares structural features with BBS1 and BBS2. *Am. J. Hum Genet., 72* (3), 650-658.

Baker, S.A., Freeman, K., Luby-Phelps, K., Pazour, G.J., & Besharse, J.C. (2003). IFT20 links kinesin II with a mammalian intraflagellar transport complex that is conserved in motile flagella and sensory cilia. *J. Biol. Chem., 278* (36), 34211-34218.

Basinger, S., Bok, D., & Hall, M. (1976). Rhodopsin in the rod outer segment plasma membrane. *J. Cell Biol., 69* (1), 29-42.

Beales, P.L., Bland, E., Tobin, J.L., Bacchelli, C., Tuysuz, B., Hill, J., Rix, S., Pearson, C.G., Kai, M., Hartley, J., Johnson, C., Irving, M., Elcioglu, N., Winey, M., Tada, M., & Scambler, P.J. (2007). IFT80, which encodes a conserved intraflagellar transport protein, is mutated in Jeune asphyxiating thoracic dystrophy. *Nat Genet., 39* (6), 727-729.

Berbari, N.F., Lewis, J.S., Bishop, G.A., Askwith, C.C., & Mykytyn, K. (2008). Bardet-Biedl syndrome proteins are required for the localization of G protein-coupled receptors to primary cilia. *Proc. Natl. Acad. Sci. U S A., 105* (11), 4242-4246.

Chen, J., Shi, G., Concepcion, F.A., Xie, G., Oprian, D., & Chen, J. (2006). Stable rhodopsin/arrestin complex leads to retinal degeneration in a transgenic mouse model of autosomal dominant retinitis pigmentosa. *J. Neurosci., 26* (46), 11929-11937.

Cole, D.G. (2003). The intraflagellar transport machinery of Chlamydomonas reinhardtii. *Traffic, 4* (7), 435-442.

Cole, D.G., Diener, D.R., Himelblau, A.L., Beech, P.L., Fuster, J.C., & Rosenbaum, J.L. (1998). Chlamydomonas kinesin-II-dependent intraflagellar transport (IFT): IFT

particles contain proteins required for ciliary assembly in Caenorhabditis elegans sensory neurons. *J. Cell Biol., 141* (4), 993-1008.

Corbit, K.C., Aanstad, P., Singla, V., Norman, A.R., Stainier, D.Y., & Reiter, J.F. (2005). Vertebrate smoothened functions at the primary cilium. *Nature, 437* (7061), 1018-1021.

Davenport, J.R., & Yoder, B.K. (2005). An incredible decade for the primary cilium: a look at a once-forgotten organelle. *Am. J. Physiol. Renal Physiol., 289* (6), F1159-1169.

De Robertis, E. (1956a). Electron microscope observations on the submicroscopic organization of the retinal rods. *J. Biophys. Biochem. Cytol., 2* (3), 319-330.

De Robertis, E. (1956b). Morphogenesis of the retinal rods. *J. Biophysic. and Biocehm. Cytol., 2*, 209-218.

De Robertis, E. (1956c). Morphogenesis of the retinal rods; an electron microscope study. *J. Biophys. Biochem. Cytol., 2,* 209-218.

De Robertis, E. (1960). Some observations on the ultrastructure and morphogenesis of photoreceptors. *J. Gen. Physiol., 43(6)*, 1-13.

Deane, J.A., Cole, D.G., Seeley, E.S., Diener, D.R., & Rosenbaum, J.L. (2001). Localization of intraflagellar transport protein IFT52 identifies basal body transitional fibers as the docking site for IFT particles. *Curr. Biol., 11* (20), 1586-1590.

Doerre, G., & Malicki, J. (2002). Genetic analysis of photoreceptor cell development in the zebrafish retina. *Mech. Dev., 110* (1-2), 125-138.

Dowling, J.E. (1970). Organization of vertebrate retinas. *Invest. Ophthalmol., 9* (9), 655-680.

Dowling, J.E. (1978). How the retina "sees." *Invest. Ophthalmol. Vis. Sci., 17* (9), 832-834.

Dowling, J.E. (1987). *The Retina: An Approachable Part of the Brain*. Cambridge, MA: Harvard University Press.

Driever, W., Solnica-Krezel, L., Schier, A.F., Neuhauss, S.C., Malicki, J., Stemple, D.L., Stainier, D.Y., Zwartkruis, F., Abdelilah, S., Rangini, Z., Belak, J., & Boggs, C. (1996). A genetic screen for mutations affecting embryogenesis in zebrafish. *Development, 123*, 37-46.

Easter, S.S., Jr., & Nicola, G.N. (1996). The development of vision in the zebrafish (Danio rerio). *Dev. Biol., 180* (2), 646-663.

Eisen, J.S. (1991). Developmental neurobiology of the zebrafish. *J. Neurosci., 11* (2), 311-317.

Fadool, J.M., & Dowling, J.E. (2008). Zebrafish: a model system for the study of eye genetics. *Prog. Retin. Eye Res., 27* (1), 89-110.

Fawcett, D.W., & Porter, K.R. (1954). A study of the fine structure of ciliated epithelia. *J. Morphol., 94*, 221.

Follit, J.A., Tuft, R.A., Fogarty, K.E., & Pazour, G.J. (2006). The intraflagellar transport protein IFT20 is associated with the Golgi complex and is required for cilia assembly. *Mol. Biol. Cell., 17* (9), 3781-3792.

Goldsmith, P., & Harris, W.A. (2003). The zebrafish as a tool for understanding the biology of visual disorders. *Semin. Cell Dev. Biol., 14* (1), 11-18.

Gouttenoire, J., Valcourt, U., Bougault, C., Aubert-Foucher, E., Arnaud, E., Giraud, L., & Mallein-Gerin, F. (2007). Knockdown of the intraflagellar transport protein IFT46 stimulates selective gene expression in mouse chondrocytes and affects early development in zebrafish. *J. Biol. Chem., 282* (42), 30960-30973.

Gross, J.M., & Perkins, B.D. (2008). Zebrafish mutants as models for congenital ocular disorders in humans. *Mol. Reprod. Dev., 75* (3), 547-555.

Gross, J.M., Perkins, B.D., Amsterdam, A., Egana, A., Darland, T., Matsui, J.I., Sciascia, S., Hopkins, N., & Dowling, J.E. (2005). Identification of zebrafish insertional mutants with defects in visual system development and function. *Genetics, 170* (1), 245-261.

Haffter, P., & Nusslein-Volhard, C. (1996). Large scale genetics in a small vertebrate, the zebrafish. *Int. J. Dev. Biol., 40* (1), 221-227.

Handel, M., Schulz, S., Stanarius, A., Schreff, M., Erdtmann-Vourliotis, M., Schmidt, H., Wolf, G., & Hollt, V. (1999). Selective targeting of somatostatin receptor 3 to neuronal cilia. *Neuroscience, 89* (3), 909-926.

Haycock, J.W., & Bro, S. (1975). Corpus striatum (Translation of S. Ramon y Cajal). translated from Corps Strie, chapter 23, in "Histologie du systeme nerveux de l'homme et des vertebres" 1911. *Behav. Biol., 14* (3), 387-402.

Haycraft, C.J., Schafer, J.C., Zhang, Q., Taulman, P.D., & Yoder, B.K. (2003). Identification of CHE-13, a novel intraflagellar transport protein required for cilia formation. *Exp. Cell Res., 284* (2), 251-263.

Haycraft, C.J., Swoboda, P., Taulman, P.D., Thomas, J.H., & Yoder, B.K. (2001). The C. elegans homolog of the murine cystic kidney disease gene Tg737 functions in a ciliogenic pathway and is disrupted in osm-5 mutant worms. *Development, 128* (9), 1493-1505.

Horst, C.J., Johnson, L.V., & Besharse, J.C. (1990). Transmembrane assemblage of the photoreceptor connecting cilium and motile cilium transition zone contain a common immunologic epitope. *Cell Motil. Cytoskeleton, 17* (4), 329-344.

Hou, Y., Qin, H., Follit, J.A., Pazour, G.J., Rosenbaum, J.L., & Witman, G.B. (2007). Functional analysis of an individual IFT protein: IFT46 is required for transport of outer dynein arms into flagella. *J. Cell Biol., 176* (5), 653-665.

Houde, C., Dickinson, R.J., Houtzager, V.M., Cullum, R., Montpetit, R., Metzler, M., Simpson, E.M., Roy, S., Hayden, M.R., Hoodless, P.A., & Nicholson, D.W. (2006). Hippi is essential for node cilia assembly and Sonic hedgehog signaling. *Dev. Biol., 300* (2), 523-533.

Hu, M., & Easter, S.S. (1999). Retinal neurogenesis: the formation of the initial central patch of postmitotic cells. *Dev. Biol., 207* (2), 309-321.

Huangfu, D., Liu, A., Rakeman, A.S., Murcia, N.S., Niswander, L., & Anderson, K.V. (2003). Hedgehog signalling in the mouse requires intraflagellar transport proteins. *Nature, 426* (6962), 83-87.

Insinna, C., Pathak, N., Perkins, B., Drummond, I., & Besharse, J.C. (2008). The homodimeric kinesin, Kif17, is essential for vertebrate photoreceptor sensory outer segment development. *Dev. Biol., 316* (1), 160-170.

Kahn, A.J. (1974). An autoradiographic analysis of the time of appearance of neurons in the developing chick neural retina. *Dev. Biol., 38* (1), 30-40.

Kolb, H. (1977). The organization of the outer plexiform layer in the retina of the cat: electron microscopic observations. *J. Neurocytol., 6* (2), 131-153.

Kolb, H., Nelson, R., & Mariani, A. (1981). Amacrine cells, bipolar cells and ganglion cells of the cat retina: a Golgi study. *Vision Res., 21* (7), 1081-1114.

Kolb, H., & West, R.W. (1977). Synaptic connections of the interplexiform cell in the retina of the cat. *J. Neurocytol., 6* (2), 155-170.

Kondo, S., Sato-Yoshitake, R., Noda, Y., Aizawa, H., Nakata, T., Matsuura, Y., & Hirokawa, N. (1994). KIF3A is a new microtubule-based anterograde motor in the nerve axon. *J. Cell. Biol., 125* (5), 1095-1107.

Kozminski, K.G., Beech, P.L., & Rosenbaum, J.L. (1995). The Chlamydomonas kinesin-like protein FLA10 is involved in motility associated with the flagellar membrane. *J. Cell. Biol., 131* (6 Pt 1), 1517-1527.

Kozminski, K.G., Johnson, K.A., Forscher, P., & Rosenbaum, J.L. (1993). A motility in the eukaryotic flagellum unrelated to flagellar beating. *Proc. Natl. Acad. Sci., USA, 90* (12), 5519-5523.

Krock, B.L., & Perkins, B.D. (2008). The intraflagellar transport protein IFT57 is required for cilia maintenance and regulates IFT-particle-kinesin-II dissociation in vertebrate photoreceptors. *J. Cell Sci., 121* (11), 1907-1915.

Lamb, J.R., Tugendreich, S., & Hieter, P. (1995). Tetratrico peptide repeat interactions: to TPR or not to TPR? *Trends Biochem. Sci., 20* (7), 257-259.

Lucker, B.F., Behal, R.H., Qin, H., Siron, L.C., Taggart, W.D., Rosenbaum, J.L., & Cole, D.G. (2005). Characterization of the intraflagellar transport complex B core: direct interaction of the IFT81 and IFT74/72 subunits. *J. Biol. Chem., 280* (30), 27688-27696.

Marmorstein, A.D. (2001). The polarity of the retinal pigment epithelium. *Traffic, 2* (12), 867-872.

Marszalek, J.R., Liu, X., Roberts, E.A., Chui, D., Marth, J.D., Williams, D.S., & Goldstein, L.S. (2000). Genetic evidence for selective transport of opsin and arrestin by kinesin-II in mammalian photoreceptors. *Cell, 102* (2), 175-187.

Mendez, A., Lem, J., Simon, M., & Chen, J. (2003). Light-dependent translocation of arrestin in the absence of rhodopsin phosphorylation and transducin signaling. *J. Neurosci., 23* (8), 3124-3129.

Mykytyn, K., Braun, T., Carmi, R., Haider, N.B., Searby, C.C., Shastri, M., Beck, G., Wright, A.F., Iannaccone, A., Elbedour, K., Riise, R., Baldi, A., Raas-Rothschild, A., Gorman, S.W., Duhl, D.M., Jacobson, S.G., Casavant, T., Stone, E.M., & Sheffield, V.C. (2001). Identification of the gene that, when mutated, causes the human obesity syndrome BBS4. *Nat. Genet., 28* (2), 188-191.

Nawrocki, L.W. (1985). *Development of the Neural Retina in the Zebrafish, Brachyodanio rerio*. Institute of Neuroscience (Eugene: University of Oregon).

Nonaka, S., Tanaka, Y., Okada, Y., Takeda, S., Harada, A., Kanai, Y., Kido, M., & Hirokawa, N. (1998). Randomization of left-right asymmetry due to loss of nodal cilia generating leftward flow of extraembryonic fluid in mice lacking KIF3B motor protein. *Cell, 95* (6), 829-837.

Odor, D.L., & Blandau, R.J. (1985). Observations on the solitary cilium of rabbit oviductal epithelium: its motility and ultrastructure. *Am. J. Anat., 174* (4), 437-453.

Pazour, G.J., Baker, S.A., Deane, J.A., Cole, D.G., Dickert, B.L., Rosenbaum, J.L., Witman, G.B., & Besharse, J.C. (2002a). The intraflagellar transport protein, IFT88, is essential for vertebrate photoreceptor assembly and maintenance. *J. Cell Biol., 157* (1), 103-113.

Pazour, G.J., Dickert, B.L., Vucica, Y., Seeley, E.S., Rosenbaum, J.L., Witman, G.B., & Cole, D.G. (2000). Chlamydomonas IFT88 and its mouse homologue, polycystic kidney disease gene tg737, are required for assembly of cilia and flagella. *J. Cell Biol., 151* (3), 709-718.

Pazour, G.J., Dickert, B.L., & Witman, G.B. (1999). The DHC1b (DHC2) isoform of cytoplasmic dynein is required for flagellar assembly. *J. Cell Biol., 144* (3), 473-481.

Pazour, G.J., & Rosenbaum, J.L. (2002). Intraflagellar transport and cilia-dependent diseases. *Trends Cell Biol., 12* (12), 551-555.

Pazour, G.J., San Agustin, J.T., Follit, J.A., Rosenbaum, J.L., & Witman, G.B. (2002b). Polycystin-2 localizes to kidney cilia and the ciliary level is elevated in orpk mice with polycystic kidney disease. *Curr. Biol., 12* (11), R378-380.

Pazour, G.J., Wilkerson, C.G., & Witman, G.B. (1998). A dynein light chain is essential for the retrograde particle movement of intraflagellar transport (IFT). *J. Cell Biol., 141* (4), 979-992.

Pazour, G.J., & Witman, G.B. (2000). Forward and reverse genetic analysis of microtubule motors in chlamydomonas. *Methods, 22* (4), 285-298.

Pedersen, L.B., Miller, M.S., Geimer, S., Leitch, J.M., Rosenbaum, J.L., & Cole, D.G. (2005). Chlamydomonas IFT172 is encoded by FLA11, interacts with CrEB1, and regulates IFT at the flagellar tip. *Curr. Biol., 15* (3), 262-266.

Perkins, B.D., Fadool, J.M., & Dowling, J.E. (2004). Photoreceptor structure and development: analyses using GFP transgenes. *Methods Cell Biol., 76*, 315-331.

Perkins, B.D., Kainz, P.M., O'Malley, D.M., & Dowling, J.E. (2002). Transgenic expression of a GFP-rhodopsin COOH-terminal fusion protein in zebrafish rod photoreceptors. *Vis. Neurosci., 19*, 257-264.

Perkins, B.D., Nicholas, C.S., Baye, L.M., Link, B.A., & Dowling, J.E. (2005). Dazed gene is necessary for late cell type development and retinal cell maintenance in the zebrafish retina. *Dev. Dyn., 233* (2), 680-694.

Perkins, L.A., Hedgecock, E.M., Thomson, J.N., & Culotti, J.G. (1986). Mutant sensory cilia in the nematode Caenorhabditis elegans. *Dev. Biol., 117* (2), 456-487.

Peterson, J.J., Tam, B.M., Moritz, O.L., Shelamer, C.L., Dugger, D.R., McDowell, J.H., Hargrave, P.A., Papermaster, D.S., & Smith, W.C. (2003). Arrestin migrates in photoreceptors in response to light: a study of arrestin localization using an arrestin-GFP fusion protein in transgenic frogs. *Exp. Eye Res., 76* (5), 553-563.

Piperno, G., & Mead, K. (1997). Transport of a novel complex in the cytoplasmic matrix of chlamydomonas flagella. *Proc. Natl. Acad. Sci., USA, 94* (9), 4457-4462.

Piperno, G., Siuda, E., Henderson, S., Segil, M., Vaananen, H., & Sassaroli, M. (1998). Distinct mutants of retrograde intraflagellar transport (IFT) share similar morphological and molecular defects. *J. Cell Biol., 143* (6), 1591-1601.

Pissios, P., Bradley, R.L., & Maratos-Flier, E. (2006). Expanding the scales: The multiple roles of MCH in regulating energy balance and other biological functions. *Endocr. Rev., 27* (6), 606-620.

Porter, M.E., Bower, R., Knott, J.A., Byrd, P., & Dentler, W. (1999). Cytoplasmic dynein heavy chain 1b is required for flagellar assembly in Chlamydomonas. *Mol. Biol. Cell, 10* (3), 693-712.

Qin, H., Diener, D.R., Geimer, S., Cole, D.G., & Rosenbaum, J.L. (2004). Intraflagellar transport (IFT) cargo: IFT transports flagellar precursors to the tip and turnover products to the cell body. *J. Cell Biol., 164* (2), 255-266.

Qin, H., Wang, Z., Diener, D., & Rosenbaum, J. (2007). Intraflagellar transport protein 27 is a small G protein involved in cell-cycle control. *Curr. Biol., 17* (3), 193-202.

Raymond, P.A., Barthel, L.K., & Curran, G.A. (1995). Developmental patterning of rod and cone photoreceptors in embryonic zebrafish. *J. Comp. Neurol., 359* (4), 537-550.

Robert, A., Margall-Ducos, G., Guidotti, J.E., Bregerie, O., Celati, C., Brechot, C., & Desdouets, C. (2007). The intraflagellar transport component IFT88/polaris is a

centrosomal protein regulating G1-S transition in non-ciliated cells. *J. Cell Sci., 120* (4), 628-637.

Rosenbaum, J.L., Cole, D.G., & Diener, D.R. (1999). Intraflagellar transport: the eyes have it. *J. Cell Biol., 144* (3), 385-388.

Rosenbaum, J.L., & Witman, G.B. (2002). Intraflagellar transport. *Nat. Rev. Mol. Cell. Biol., 3* (11), 813-825.

Sanderson, M.J., & Sleigh, M.A. (1981). Ciliary activity of cultured rabbit tracheal epithelium: beat pattern and metachrony. *J. Cell Sci., 47*, 331-347.

Schmitt, E.A., & Dowling, J.E. (1994). Early eye morphogenesis in the zebrafish, Brachydanio rerio. *J. Comp. Neurol., 344* (4), 532-542.

Schmitt, E.A., & Dowling, J.E. (1996). Comparison of topographical patterns of ganglion and photoreceptor cell differentiation in the retina of the zebrafish, Danio rerio. *J. Comp. Neurol., 371* (2), 222-234.

Schmitt, E.A., & Dowling, J.E. (1999). Early retinal development in the zebrafish, Danio rerio: light and electron microscopic analyses. *J. Comp. Neurol., 404* (4), 515-536.

Snow, J.J., Ou, G., Gunnarson, A.L., Walker, M.R., Zhou, H.M., Brust-Mascher, I., & Scholey, J.M. (2004). Two anterograde intraflagellar transport motors cooperate to build sensory cilia on C. elegans neurons. *Nat. Cell Biol., 6* (11), 1109-1113.

Strauss, O. (2005). The retinal pigment epithelium in visual function. *Physiol. Rev., 85* (3), 845-881.

Sun, Z., Amsterdam, A., Pazour, G.J., Cole, D.G., Miller, M.S., & Hopkins, N. (2004). A genetic screen in zebrafish identifies cilia genes as a principal cause of cystic kidney. *Development, 131* (16), 4085-4093.

Sung, C.H., Davenport, C.M., Hennessey, J.C., Maumenee, I.H., Jacobson, S.G., Heckenlively, J.R., Nowakowski, R., Fishman, G., Gouras, P., & Nathans, J. (1991). Rhodopsin mutations in autosomal dominant retinitis pigmentosa. *Proc. Natl. Acad. Sci., USA, 88* (15), 6481-6485.

Tam, B.M., Moritz, O.L., Hurd, L.B., & Papermaster, D.S. (2000). Identification of an outer segment targeting signal in the COOH terminus of rhodopsin using transgenic Xenopus laevis. *J. Cell. Biol., 151* (7), 1369-1380.

Tobin, J.L., & Beales, P.L. (2007). Bardet-Biedl syndrome: beyond the cilium. *Pediatr. Nephrol., 22* (7), 926-936.

Tsujikawa, M., & Malicki, J. (2004). Intraflagellar transport genes are essential for differentiation and survival of vertebrate sensory neurons. *Neuron, 42* (5), 703-716.

Tynan, S.H., Gee, M.A., & Vallee, R.B. (2000). Distinct but overlapping sites within the cytoplasmic dynein heavy chain for dimerization and for intermediate chain and light intermediate chain binding. *J. Biol. Chem., 275* (42), 32769-32774.

Walther, Z., Vashishtha, M., & Hall, J.L. (1994). The Chlamydomonas FLA10 gene encodes a novel kinesin-homologous protein. *J. Cell Biol., 126* (1), 175-188.

Westerfield, M. (1995). The Zebrafish Book. (Eugene, OR: University of Oregon Press.
Yamazaki, H., Nakata, T., Okada, Y., & Hirokawa, N. (1995). KIF3A/B: a heterodimeric kinesin superfamily protein that works as a microtubule plus end-directed motor for membrane organelle transport. *J. Cell Biol., 130* (6), 1387-1399.

Yoder, B.K., Hou, X., & Guay-Woodford, L.M. (2002). The polycystic kidney disease proteins, polycystin-1, polycystin-2, polaris, and cystin, are co-localized in renal cilia. *J Am. Soc. Nephrol., 13* (10), 2508-2516.

Young, R.W. (1967). The renewal of photoreceptor cell outer segments. *J. Cell Biol., 33* (1), 61-72.

Young, R.W. (1971). Shedding of discs from rod outer segments in the rhesus monkey. *J. Ultrastruct. Res., 34* (1), 190-203.

Young, R.W. (1985). Cell differentiation in the retina of the mouse. *Anat. Rec., 212* (2), 199-205.

VITA

Name: Sujita Sukumaran

Address: c/o Dr. Brian Perkins,
3258 Department of Biology
College Station, Texas 77843-3258

Email Address: s.sujita@gmail.com

Education: B.S. Biological Sciences, BITS, Pilani, 2006.

M.S., Biology, Texas A&M University, 2008.